Ocean Engineering 283 (2023) 115053

Contents lists available at ScienceDirect

Ocean Engineering

journal homepage: www.elsevier.com/locate/oceaneng

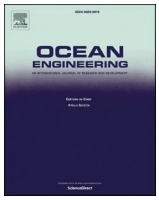

Multivariate assessment of port operability and downtime based on the wave-induced response of moored ships at berths

Eva Romano-Moreno *, Gabriel Diaz-Hernandez, Antonio Tomás, Javier L. Lara

IHCantabria - Instituto de Hidráulica Ambiental de la Universidad de Cantabria, Santander, Spain

ARTICLE INFO

Keywords:
Port operability
Moored ship system response
Numerical calibration
Wave-ship numerical coupling
Ship motion types
Mooring plan

ABSTRACT

A methodology for a multi-process and multi-variable assessment of port operability/downtime in harbors, based on the historical characterization of the wave-induced response of moored ship systems at berths, in relation to both the historical outer- and in-port spectral wave climate, is presented in this paper. A joint numerical modeling and statistical approach is adopted with the objectives of exhaustive evaluation of port operability, uncertainty bounding and computational efficiency. First, the most accurate numerical configuration to predict the multivariate response of the moored ships is determined from an extensive catalog. This is done through a prototype-data-based performance assessment, where the complete time and spectral distributions of motion variables are used, instead of the classical time-averaged or spectrum-aggregated parameterizations. Secondly, an efficient assessment of port operability/downtime and safety is achieved based on a multivariate system response pattern-type approach related to representative wave climate conditions. This multi-process characterization allows to identify specific wave climate and mooring conditions triggering downtime or unsafe situations at berths. In addition, a tailor-made mooring plan can be suggested for each situation, also visualizing the operability and safety levels relative to each system response variable. Finally, a further characterization based on joint probability functions of motion amplitudes and periods over the berthing event's duration is proposed, showing the time variability of motion variables, and suggesting advancing beyond the classical monoparametric definitions.

1. Introduction

The performance of port operations at berths is highly conditioned by the dynamic response of the moored ship system under the action of different agents, mainly the local met-ocean forcings (e.g., waves, wind, currents and sea level). Limitation or even downtime of loading/unloading, embarking/disembarking operations during a berthing event may occur due to the incompatibility of operability, efficiency and safety with excessive moored ship motions in six degrees of freedom (6 DoF). Even the exceedance of the maximum admissible loads on the mooring/fendering elements may force the ship to leave the berth (Puertos del Estado, 2012). Therefore, an adequate characterization of the dynamic response of the berthed ship system is required for a proper port operability (referring to the degree of compliance with the requirements and conditions to perform the normal operations of use and exploitation) and downtime assessment. In this way, highly multidimensional and scenario-dependent elements and processes are involved in this problem (MarCom Working Group, 2012; Molina-Sanchez et al., 2020; Pinto et al., 2008). That is, the specific features of the ship, mooring system and the harbor and berthing environment determines the multivariate response of a moored ship system to the local met-ocean forcings at berth, which, in turn, are the result of a complex interaction of the characteristic outer-harbor met-ocean conditions with the particular harbor configuration. Therefore, due to the high dimensionality and site-specificity of the problem, comprehensive multi-process analyses are required for port operability assessment.

Numerical modeling is the most widely used approach today to solve the dynamic response of moored ship systems subjected to met-ocean forcings. It usually consists of a chain of coupled numerical models aimed at serially solving the relevant processes involved (Bhautoo, 2017; Bingham, 2000; Christensen et al., 2008; de Bont et al., 2010; Drimer et al., 2000; Kwak et al., 2012; Pinheiro et al., 2012, 2013a, 2013b, 2016; Pinto et al., 2008; Terblanche and Van Der Molen, 2013; van der Molen, 2006; van der Molen and Wenneker, 2008; Wenneker

* Corresponding author.
E-mail addresses: eva.romano@unican.es (E. Romano-Moreno), gabriel.diaz@unican.es (G. Diaz-Hernandez), antonio.tomas@unican.es (A. Tomás), jav.lopez@unican.es (J.L. Lara).

https://doi.org/10.1016/j.oceaneng.2023.115053
Received 23 March 2023; Received in revised form 29 May 2023; Accepted 6 June 2023
Available online 19 June 2023

et al., 2006), through the following general three-step procedure commonly adopted: 1) offshore wave climate propagation and penetration into the harbor towards the target berthing area, disregarding the presence of the ship, by means of wave numerical models based on the elliptic mild-slope or Boussinesq equations; 2) linearized analyses of wave–freely-floating ship interaction by means of 3D diffraction/radiation potential theory-based panel models in frequency or time domain; 3) dynamic mooring analysis in time domain including the nonlinear aspects involved in the evaluation of the dynamic response of the moored ship systems. The ability to analyze a much larger number of scenarios is the main advantage of numerical modeling over other approaches, such as physical modeling or prototype monitoring campaigns. However, the commonly used approach for the coupling between the numerical wave and 3D ship panel models consists of a direct connection of the incident wave conditions defined at the panel centroid positions (Bingham, 2000; van der Molen, 2006; van der Molen and Wenneker, 2008; Wenneker et al., 2006). This means the full chain of numerical models run for each analysis simulation, with the consequent computational cost demanded given the exhaustiveness usually required for a proper characterization of the moored ship response. In addition, the need for a large amount of information for the proper model configuration and forcing, upon which the quality of the numerical prediction depends, is a major drawback of this approach. Indeed, such important required information, whether about the ship (e.g., loading condition or draft evolution during the berthing event, relative position, etc.), berth, mooring/fendering systems (e.g., mooring arrangement, pretension, elastic properties, load-elongation or deflection curves, etc.) and/or met-ocean forcings (e.g., wind, wave or current characteristics), is often unknown due to lack of actual records, difficulty of measurement or time variations. All these site-specific parameters highly determine the response of moored ship systems (Akiyama et al., 2017a,b; Rosa-Santos et al., 2014; Rosa-Santos and Taveira-Pinto, 2013; Sakakibara and Kubo, 2008a; Weiler and Dekker, 2003; Yoneyama et al., 2004), however, due to their unavailability, hypothetical or standard values have to be assumed for numerical modeling, which often leads to significant levels of uncertainty and the requirement for calibration and validation processes. At this point, both physical modeling (Abdelwahab et al., 2021; Cornett et al., 2012; Pinto et al., 2008; Rosa-Santos and Taveira-Pinto, 2013; Rosa-Santos et al., 2014; Shi, 2018; Yan, 2014) and prototype monitoring (Alvarellos et al., 2021; Costas et al., 2022a, 2022b; Figuero et al., 2018; Jensen et al., 1990; Li and Qiu, 2016; López and Iglesias, 2014; Sakakibara and Kubo, 2008b; Sande et al., 2019; Trejo et al., 2014; Uzaki et al., 2010) approaches may play a crucial role. However, the calibration processes of highly multidimensional problems, such as the current study, may often be laborious and even hardly conclusive. These may be some of the reasons why, in common practice, the long-term assessment of port operability at berths is not usually based on characterizing the complete statistics of the moored ship response. Instead, single event- and specific problem-based approaches addressing port operability and downtime at berths are more commonly adopted (Abdelwahab et al., 2021; Bhautoo, 2017; Costas et al., 2022a; de Bont et al., 2010; Figuero et al., 2019; Pinto et al., 2008; Rosa-Santos and Taveira-Pinto, 2013; Sakakibara and Kubo, 2008a). Alternatively, in the assessment of port operability/downtime levels, the probability of exceedance of recommended operational ship motion thresholds is often related to the probability of occurrence of the corresponding met-ocean forcing parameters (Kwak and Pyunan, 2014; Prpić-Oršić et al., 2014; Sakakibara and Kubo, 2008a) using typical monoparametric approaches.

In this paper, progress is made towards an exhaustive, long-term statistical assessment of port operability and downtime at berths, through a multi-process and multi-variable evaluation based on the historical characterization of the wave-induced response of moored ship systems at berths, in relation to both the historical outer- and in-port spectral wave climate. In this way, a comprehensive description of all the processes involved is provided, from the local wave forcing agents, their multidimensional interaction with the port structures and the ship, to the final induced response of the moored ship system. To achieve this ultimate goal, a joint numerical modeling and statistical approach is adopted, where, in addition, two important aspects should be highlighted: computational efficiency, and minimization or bounding of uncertainty associated with numerical modeling. First, a more computationally efficient approach than those usually applied is used, based on a single panel model calculation that provides a normalized coupling between the wave and the time domain moored ship response numerical models, which is applicable in all analysis situations. Secondly, the problem of uncertainty introduced by the unavailability of relevant information is addressed. In this regard, two main sources of uncertainty are considered. On the one hand, a key point that conditions the quality of the modeling is the accuracy in defining the local forcing agents at berths. In this work, an improved definition of the spectral wave agitation (also referred to as harbor tranquility) conditions is used to

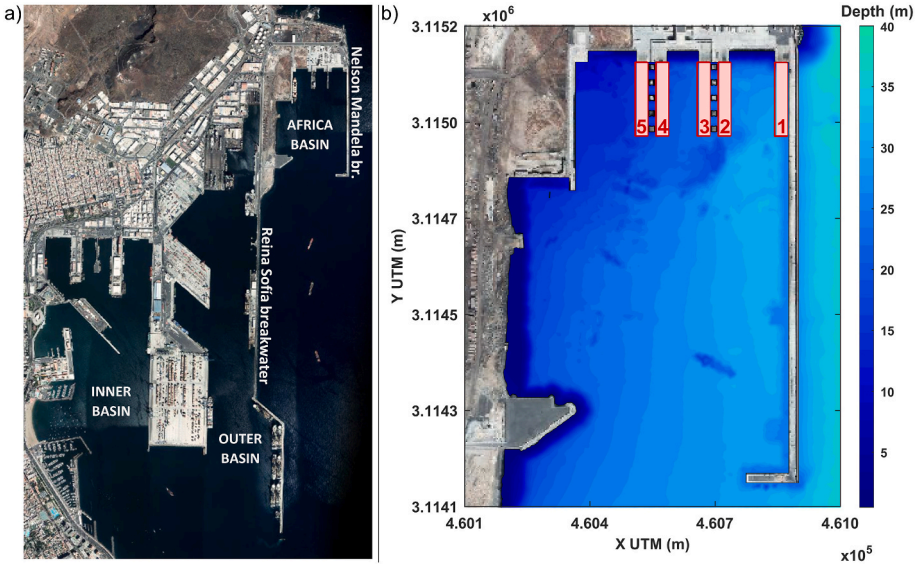

Fig. 1. a) Location of Africa basin in Las Palmas Port. Actual port geometry. Source of base map (ortophoto of 2019): viewfinder Grafcan (IDE Canarias, Government of the Canary Islands). b) Location of the RoPax-Ferry terminal and the specific Berth 3 in Africa basin. UTM coordinates (m). Actual bathymetry (m).

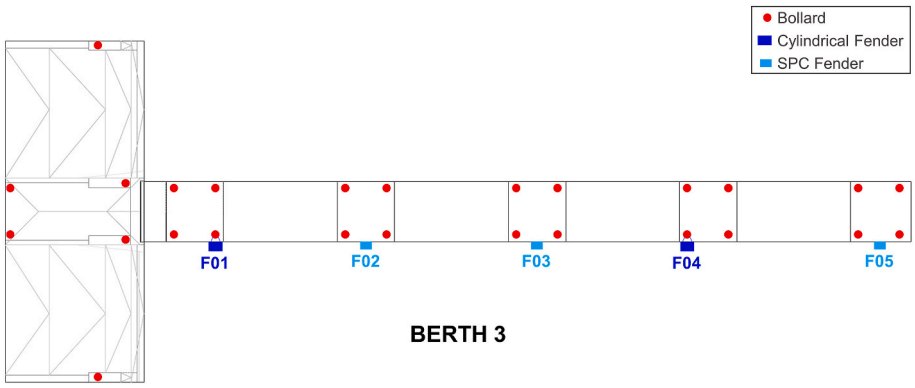

Fig. 2. Layout of Berth 3 (rotated 90° counterclockwise from its actual orientation). Position of bollards and fenders.

force the moored ship model, compared to the theoretical unimodal definitions and standard parameterizations commonly used (Abdelwahab et al., 2021; Christensen et al., 2008; de Bont et al., 2010; Kwak and Pyunan, 2014; Rosa-Santos et al., 2014; Rosa-Santos and Taveira-Pinto, 2013; Sakakibara and Kubo, 2008a; van der Molen, 2006; van der Molen and Wenneker, 2008). On the other hand, an advanced multivariate performance analysis based on comparison with prototype data, both in the time and frequency domain, is performed with the objective of identifying the most accurate numerical configuration of the unknown mooring and fendering system from an extensive catalog to predict the multivariate response of the study moored ship.

Finally, a further step is taken to reach the final objective. An effective characterization of port operability and downtime at berths is achieved through a practical approach based on multivariate system response pattern-types, including ship motions and forces on mooring lines, related to each representative historical outer- and in-port wave climate condition. This improved characterization may be a relevant aspect for both port operability/downtime and safety assessment, allowing the suggestion of the most convenient mooring plan (among those analyzed) for each representative wave climate condition, as well as the identification of specific wave climate and mooring conditions triggering downtime and even unsafe situations, such as line breakage. It is important to note that a detailed description based on the entire time series characterization underlies this representative pattern-type definition. In this way, a further characterization in terms of joint probability functions of motion amplitude and period parameters, beyond single-value statistical parameters, is proposed.

This paper is organized as follows: Materials and methods are presented in Section 2. Section 2.1 presents the study case of moored ship at berth where the proposed methodology is applied. The prototype measured data used in the calibration and validation procedures are also described. A brief characterization of the historical multimodal wave agitation/harbor tranquility climate in the study berth is presented in Section 2.2. In Section 2.3, the methodology is described in separate steps. Section 3 presents the results and discussion. The methodology is applied and tested with prototype measured data for different berthing events in the study case. An efficient port operability/downtime assessment based on the proposed multi-process characterization is presented. The discussion of the proposed methodology and the results is included. The main conclusions are summarized in Section 4.

2. Material and methods

2.1. Study case

The Africa basin is in Las Palmas Port, which is on the northeast tip of Gran Canaria Island in Spain. This basin is facing the Atlantic Ocean, with the port entrance open on the southern side (as shown in Fig. 1). The main sheltering structure is the Nelson Mandela breakwater, which bounds the eastern side of the basin. It is 1000 m long, approximately, with a concrete caisson-made vertical cross section. The western boundary contour of the basin is the Reina Sofia breakwater, which is approximately 3000 m long, with a rubble mound cross section in the first 1600 m, and a vertical caisson cross section in the final 1400 m. Vertical quay wall is the predominant typology of inner contours of the basin, except for the north contour, where sloped rubble mound typology exists between concrete berthing ramps.

Table 1
Main characteristics of the "Volcán del Teide" ferry (Hijos de J.Barreras, 2015).

Length overall	171.55 m
Length between perpendiculars	159.00 m
Moulded Breadth	26.40 m
Depth to main Deck	9.50 m
Design Moulded Draught	6.40 m
Deadweight at draught 6.40 m	4850 t

A RoPax-Ferry terminal consisting of five berths is located on the northeast part of the basin (Fig. 1b). Berth 3 is the focus of this research and has been selected because it was the most frequent berthing area of the monitored ship during the prototype measurement campaign used in this work. The berthing structure is a double-side pier of 166 m long and 13 m wide, formed by five discontinuously-placed vertical caissons joined by a concrete deck, in a north-south orientation. Berth 3 is located on the western side of the pier. The mean water depth along the berthing area is 21.4 m (referred to Low Water Level, LWL = 0.0 m; Fig. 1b). The maximum tidal range is 3.0 m.

Berth 3 is equipped with five fenders, one per vertical caisson, arranged as follows: the fenders on the first and fourth caissons (F01 and F04 in Fig. 2) are rubber cylindrical fenders hanging from bollards, while the fenders on the rest of the caissons (F02, F03 and F05) are SPC (Super Circle) type fenders installed centered on the caissons' walls. The position of bollards fitted on the superstructure is shown in Fig. 2.

The ship studied in this work is a RoPax type ("Volcán del Teide" ferry), operated by Naviera Armas. The main characteristics of the ship are summarized in Table 1. According to the mooring arrangement plan, the mooring lines are polysteel ropes. On-site measurements revealed diameters between 64 and 75 mm.

A tailor-made field campaign was defined within the Africa basin to measure both the met-ocean variables and the dynamic moored ship response. On-site measurements have been used for numerical calibration and validation tasks of in-port wave agitation and dynamic moored ship response of the "Volcán del Teide" ferry. A multi-position scalar and directional validation of the numerical wave agitation prediction within the port basin, based on the comparison with on-site wave agitation measured data, is presented in Romano-Moreno et al. (2022, 2023). The information on the moored ship response measured during one month

Table 2
Date and duration for the monitored berthing events of the "Volcán del Teide" ferry moored at Berth 3. Range of numerically obtained wave parameter values (zero-order moment spectral wave height, Hm_0; peak period, Tp; mean wave direction, Dm) for the main ($_1$) and secondary ($_2$) spectral wave agitation components at the position of the moored ship's center of gravity, wind parameters and sea level. The hourly minimum and maximum values of the met-ocean parameters during the events are indicated.

Berthing event			Wave agitation						Wind		Sea level (m)
#	Date	Dur.	Hm_{0_1} (m)	$Tp_{\_1}$ (s)	$Dm_{\_1}$ (°)	Hm_{0_2} (m)	$Tp_{\_2}$ (s)	$Dm_{\_2}$ (°)	Vw (m/s)	Dw (°)	
A	03/02/20; 19:00–23:00	5 h	[0.25, 0.29]	[4.6, 4.9]	S	[0.11, 0.15]	5.0	E	[2.6, 5.5]	[E, ESE]	[1.77, 1.97]
B	04/02/20; 17:00–23:00	7 h	[0.26, 0.40]	[4.8, 5.3]	S	[0.15, 0.23]	[5.0, 5.1]	E	[2.2, 4.6]	[NNE, E]	[1.23, 2.06]
C	10/02/20; 19:00–23:00	5 h	[0.24, 0.27]	[5.1, 8.3]	S	[0.19, 0.26]	[5.0, 15.0]	S	[4.4, 6.2]	SSE	[0.49, 1.43]
D	11/02/20; 16:00–23:00	8 h	[0.24, 0.26]	[16.1, 17.0]	S	[0.22, 0.24]	[4.8, 5.0]	S	[3.8, 4.9]	SE	[0.49, 2.56]
E	18/02/20; 17:00–23:00	7 h	[0.46, 0.69]	[8.5, 8.6]	S	[0.30, 0.36]	[5.2, 16.9]	S	[7.9, 8.6]	SSE	[1.18, 2.15]

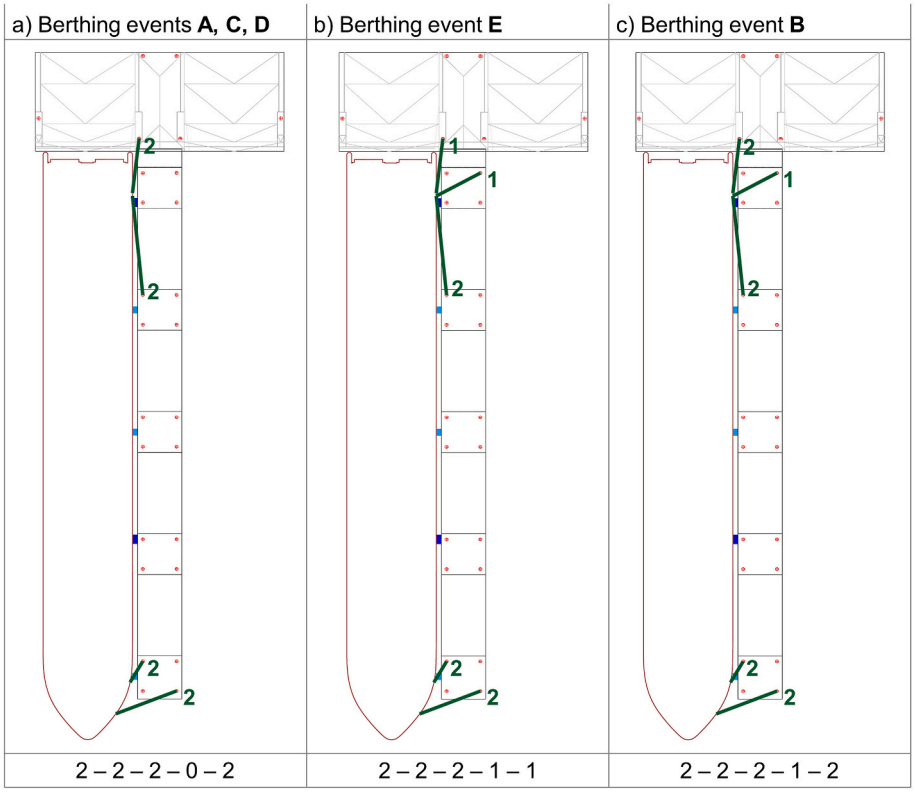

Fig. 3. Mooring plans corresponding to the monitored berthing events A, B, C, D and E, along with the number of lines per bollard. Lines are defined as follows: head lines – fore spring lines – aft spring lines – aft breast lines – stern lines.

(February 2020) is used. An IMU (Inertial Measurement Unit) sensor was installed in the "Volcán del Teide" ferry during the field campaign. The rotational motions (roll, pitch and yaw) and accelerations on the three axes (X, Y and Z) were measured, with a maximum sample rate of 100 Hz, during the field campaign. Additionally, time series of displacements on the three axes (surge, sway and heave) were calculated. In this way, the time series of nine variables (3-axes displacements, rotations and accelerations) for the duration of each berthing event are available for comparison, calibration and validation of the numerical model.

During the 1-month field campaign, a total of 5 berthing episodes (32 h; see Table 2) were recorded for the "Volcán del Teide" ferry moored at Berth 3. The actual mooring plans for each berthing event were also registered (see Fig. 3, where the arrangement and the number of mooring lines per bollard are presented). The met-ocean conditions numerically obtained at the position of the ship's center of gravity (see Section 2.3.1) during each event are summarized in Table 2.

2.2. Multimodal wave agitation climate in the study berth

A highly multimodal wave climate prevails in the vicinity of Africa basin. The predominant outer-harbor wave climate conditions come from NNE wave directions, with peak periods (Tp) between 5 and 15 s. Two different processes of outer-harbor NE wave energy penetration into the Africa basin are identified: 1) wave diffraction at the port entrance; 2) wave energy reflection on the Reina Sofia breakwater towards the eastern inner half of the basin. In addition, outer-harbor SE waves with Tp mainly between 5 and 7.5 s are also present in the study area although with lower probability of occurrence. Due to the orientation of the port entrance, these SE wave components directly impact the western inner half of the basin, from where they are reflected to the rest of the port basin (Romano-Moreno et al., 2022, 2023). Because of Berth 3's almost central position in the African basin, it is highly exposed to the entering wave energy through these three wave penetration processes and several wave reflections on the in-port contours. This is illustrated in Fig. 4b, where two representative wave agitation spectral types (ST; based on Romano-Moreno et al. (2023)), corresponding to

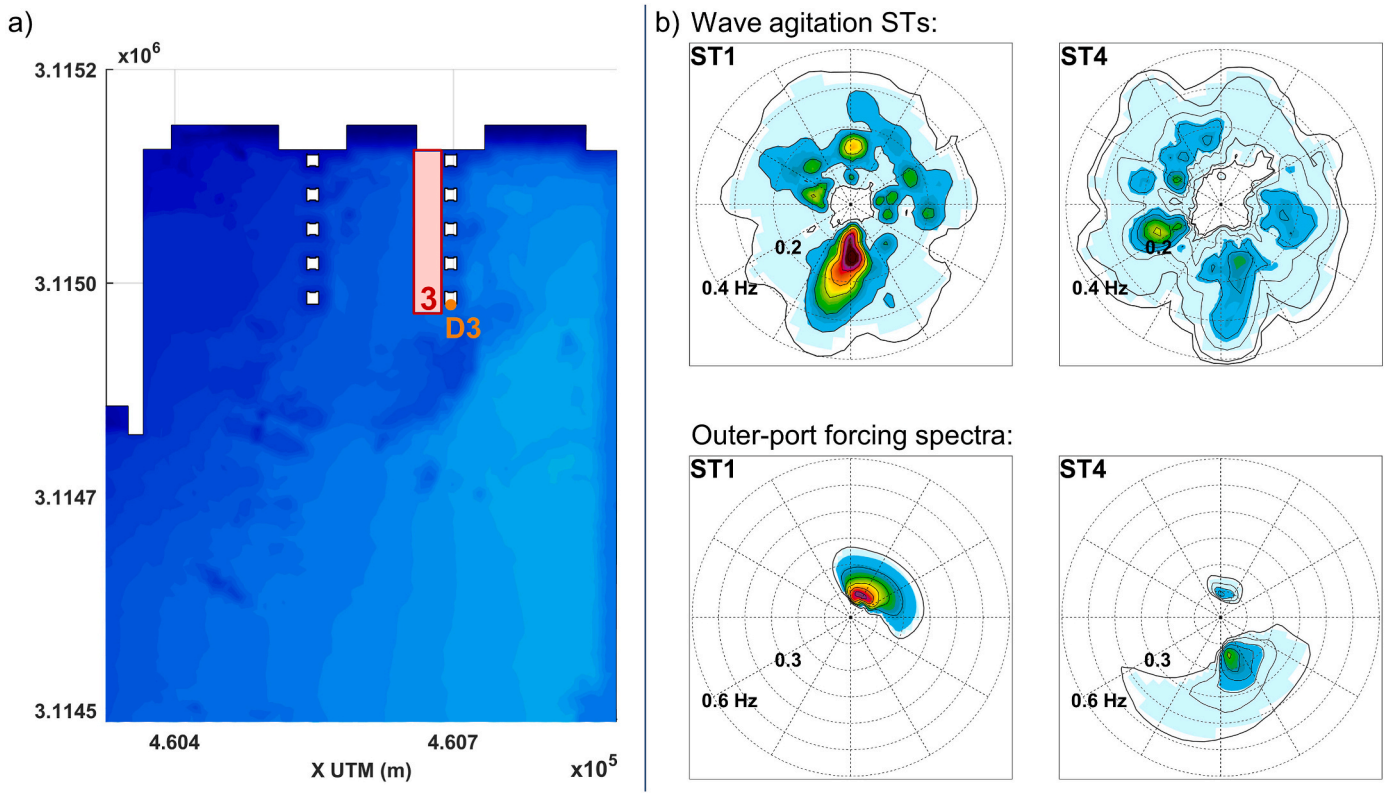

Fig. 4. a) Location of Berth 3 and control point D3 in Africa basin. b) Sample wave agitation spectral types at point D3; Outer-port forcing spectra corresponding to each wave agitation ST.

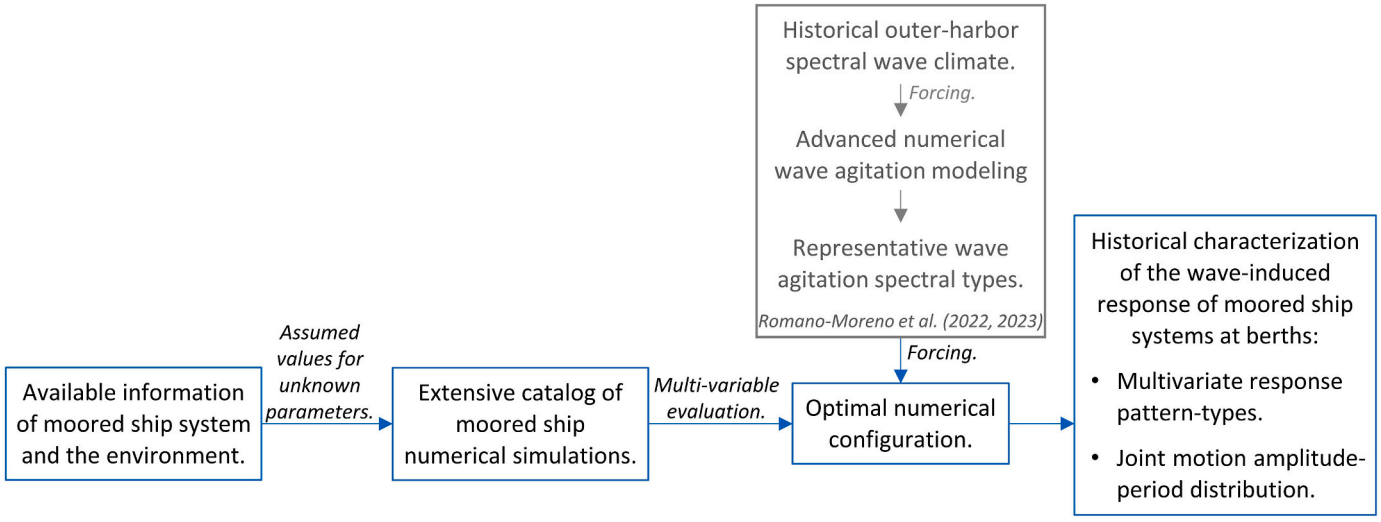

Fig. 5. Overall methodology framework.

outer-port forcing spectra with the primary wave energy components coming from NE and SSE directions, respectively, are shown for a position in front of the target berthing structure (point D3; Fig. 4a). The south-oriented wave components in the wave agitation STs corresponds to the penetrating wave energy into the basin. The in-port reflected waves are shown as wave energy components from WSW to ESE directions (clockwise) in both STs.

2.3. Methodology

The overall methodology framework proposed for a multi-process and multivariate assessment of port operability is presented in Fig. 5. As a general description, attaining a numerical configuration to model the response of the moored ship in the study case, dealing with the lack of some determining information, is firstly sought in the methodology. Once the final numerical setup is defined, the main objective of achieving a comprehensive, long-term statistical assessment of port operability at berths is addressed.

2.3.1. Numerical modeling

SHIP-MOORINGS (Arcadis, 2016a) is the numerical model used in this work. This model solves the equation of motion (6 DoF) in time

domain, including the nonlinear aspects involved in evaluating the dynamic response of the moored ship system based on the impulse response function-based formulation (Eq. (1)) proposed by Cummins (1962).

$$F_k(t) = \sum_{j=1}^{6}\left[\left(M_{kj}+m_{kj}\right)\ddot{x}_j + \int_{-\infty}^{t} K_{kj}(t-\tau)\,\dot{x}_j(\tau)\,d\tau + C_{kj}x_j\right] \quad (1)$$

where F_k represents all the time-varying external forces acting on the ship; x_j is the ship motion in j direction (with $j = 1$ to 6 for each DoF); M_{kj} is the inertia matrix of the ship; m_{kj} is the constant frequency-independent added mass coefficient matrix, associated with the inertial effects of the surrounding water due to the instantaneous ship acceleration (impulsive/instantaneous force contribution); C_{kj} is the hydrostatic restoring force coefficient matrix; τ is the time shift; and K_{kj} is the matrix of retardation functions accounting for the forcing contribution at time t due to the past history (convolution integral) of the ship motions (Arcadis, 2016a; Bingham, 2000; Cummins, 1962; Duarte, 2013; Lewandowski, 2004; Van Oortmerssen, 1976; Wichers, 1988). For the previous hydrodynamic computations in frequency domain, the 3D potential theory-based panel model DIFFRAC (Maritime Research Institute Netherlands, 2010; Van Oortmerssen, 1976) has been used. The actual 3D geometry of the berthing structure (vertical caissons, concrete ramps and lateral slopes extended to approximately 500 m on each side) and the ship's hull have been defined in DIFFRAC.

The numerical strategy followed in this work is not based on a direct coupling between the wave agitation model, the 3D panel model and the time domain moored ship model for each numerical simulation. Otherwise, a more computationally efficient approach is adopted, based on a single panel model calculation providing a normalized coupling between the wave and the time domain moored ship response numerical models. It is applicable in all analysis situations since this computation has been performed as a wave frequency-direction sweep covering all the expected wave climate conditions in the berthing area. The forcing wave conditions at specific positions (typically, the ship's center of gravity, CoG) are used to force the wave-induced moored ship response. At this point, the proper definition of these forcing wave conditions plays an important role. Based on the frequency-direction wave agitation spectra definition presented in Romano-Moreno et al. (2023), a disaggregated spectral characterization of the forcing wave conditions used to force the SHIP-MOORINGS model is obtained. This is a computationally efficient numerical approach to be adopted in an iterative calibration procedure of the moored ship numerical model, such as the current study. Since a discontinuous berthing structure is addressed in this study, transformation processes of waves passing through the vertical caissons towards the ship's CoG location occur. These effects, as well as wave reflection on port structures defined in DIFFRAC computations, have already been modeled in the panel model. Thus, the forcing incident wave conditions are defined accordingly in SHIP-MOORINGS model. Prior to the moored ship model, the directional wave agitation spectra at the target positions have been estimated following the numerical wave agitation approach described in Romano-Moreno et al. (2023). The different incident wave systems acting on the moored ship are separately characterized from the directional spectra partitioning (MetOcean Solutions Ltd., 2018; Hanson et al., 2009). The actual frequency spectrum and spectral parameters, including directional spreading, are specified in SHIP-MOORINGS. Three random (but reproducible) simulations of irregular wave signals have been performed per case, i.e, the same three initially random start seed numbers have been used in all the simulated cases in this study in order to obtain fully comparable results. Slowly-varying drift forces (Pinkster, 1980; Arcadis, 2016b) have been included in the simulations. Input wind conditions at 10 m height have been defined from the Climate Forecast System (CFSv2) (Saha et al., 2014) wind fields. Spectral and directional variable wind conditions according to Simiu and Scanlan (1996) are reproduced in SHIP-MOORINGS. Total sea level values (astronomical tide and storm surge) have been determined from Global Ocean Tide (GOT) (IHCantabria reconstruction based on the TPXO global tides model (Egbert et al., 1994; Egbert and Erofeeva, 2002)) and Global Ocean Surges (GOS) (Cid et al., 2014) datasets. The infragravity wave phenomenon has not been included in this analysis since the study basin does not experience the unfavorable infragravity-resonance effects, and no such wave energy has been observed in the frequency spectra obtained from the wave gauges installed during the field campaign in the basin. In this study, each berthing hour has been separately analyzed. Therefore, the corresponding hourly forcings for each of the 32 berthing hours analyzed have been considered in the numerical simulations.

Table 3
Range of values assumed for the unknown parameters in the different numerical setups numerically modeled.

Parameter	Assumed values
Diameter of mooring lines (mm)	64, 68, 72, 75
Initial pretension of mooring lines (kN)	0, 20, 30, 50, 60, 70, 100, 120, 150, 180, 200
Load – elongation curve of mooring lines	Higher/lower elasticity; new/used
Hysteresis effects on fenders (%)	0, 10, 20
Z coordinate of hanging cylindrical fenders (m)	Z coordinate in drawings ± 0.5 m

The actual mooring plans registered during the monitoring campaign have been introduced in SHIP-MOORINGS. However, due to the lack of specific information about other features of the mooring and fendering system, an extensive catalog has been created with various numerical configurations to be analyzed numerically, in order to properly determine such absent and relevant information. A total of 648 different configurations have been defined as different combinations of the following unknown (and subject to change) parameters: diameter, load-elongation curve and pretension of mooring lines, hysteresis effects on fenders and Z coordinate of cylindrical hanging fenders (F01 and F04; Fig. 2). The different values assumed for the different configurations are presented in Table 3. These aspects have been taken into account for the analysis because of their important influence on the expected response of the moored ship (Akiyama et al., 2017a,b; Rosa-Santos et al., 2014; Rosa-Santos and Taveira-Pinto, 2013; Sakakibara and Kubo, 2008a; Weiler and Dekker, 2003; Yoneyama et al., 2004). Performance curves and other characteristics (e.g. MBL or friction) of mooring lines and fenders have been defined according to catalog specifications and guidelines.

Finally, 3-h simulations have been performed per hourly case (i.e., per berthing hour). In this way, 9 random sea states (3 random seeds × 3-h duration) have been analyzed for each numerical configuration in the catalog and each of the 32 berthing hours. A time step of 0.2 s has been defined, consistent with the time increment in the prototype measured time series.

2.3.2. *Identification of the optimum set of unknown parameters*

The aim of this analysis is to identify the optimal numerical configuration that yields the most accurate prediction of the multivariate moored ship response in the study case, from the catalog of numerical simulations performed. A twofold evaluation is carried out, in both time and frequency domain, of the behavior of the numerical system in each scenario compared to on-site prototype measurements. In contrast to the typical time-averaged or spectrum-aggregated approaches, the comparison is made in terms of the complete time and spectral distributions from the entire motion and acceleration signals.

2.3.2.1. Time domain analysis. First, a zero up-crossing analysis is performed to calculate the series of some characteristic parameters from all the numerical and measured signals of ship motions and accelerations (accs). The following zero up-crossing parameters are considered: peak-to-peak ($H_{P\text{-}P}$), positive and negative zero-to-peak amplitudes ($A_{Z\text{-}P}$) and

period between two consecutive zero up-crossings ($T_{Z\text{-}Z}$). Thus, the moored ship response for each berthing hour is characterized by 27 series of parameters ([$H_{P\text{-}P}$, $A_{Z\text{-}P}$, $T_{Z\text{-}Z}$] × [6 DoF + 3 accs]) calculated from the corresponding monitored data and as many from each numerical simulation.

Then, the performance of each numerical setup is evaluated in terms of similarity between model- and measurement-based Probability Density Functions (PDFs) of $H_{P\text{-}P}$, $A_{Z\text{-}P}$ and $T_{Z\text{-}Z}$, calculated as binned histograms. Bin widths of 0.05 m (or °), and 0.025 m/s^2 have been defined for $H_{P\text{-}P}$ and $A_{Z\text{-}P}$ PDFs of motions and accelerations, respectively. Bin widths of 2.5 s and 1.5 s have been defined for $T_{Z\text{-}Z}$ PDFs of motions and accelerations, respectively. The mean numerical PDFs are calculated from the corresponding specific PDFs obtained for each random seed-based simulation.

The Bhattacharyya coefficient (BHA, Eq. (2); Bhattacharyya, 1943; Masanganise et al., 2014) is used to evaluate the numerical prediction skill. It measures the amount of overlap between two data samples characterized by their probability distribution (represented by the proportion of counted data per histogram bin).

$$BHA = \sum_{i=1}^{k} \sqrt{p_n(i) \cdot p_m(i)} \tag{2}$$

where p_n and p_m are the probability per bin in the numerical and measurement histograms, respectively; $i = 1, \ldots k$ indicates histogram bins.

To obtain an all-in-one index for evaluating the multivariate prediction skill, joint BHA coefficients are used by concatenation of the 27 PDFs involved per case. Joint BHA ranges from 0 to 1, indicating no overlap and total overlap, respectively.

2.3.2.2. Frequency domain analysis. In this analysis, the frequency spectra of all motion and acceleration signals are obtained for comparison. In this way, the moored ship response for each berthing hour is characterized by 9 spectral curves (6 DoF + 3 accs) calculated from the corresponding monitored data and as many from each numerical simulation. The WAFO toolbox (Brodtkorb et al., 2000; WAFO-group, 2000) has been used to calculate the hourly frequency spectra from time series. The same segment length is used for the spectral analysis of measured and numerical signals. Spectral values above 0.33 Hz have been disregarded because no spectral values are obtained at these frequencies for numerical model-based spectra. The small energy contribution of these components into the total energy for measurement-based spectra is considered as noise. In addition, for consistency with the wave forcing used in the numerical ship model, since wave frequencies above such frequency value were not propagated in the wave agitation modeling (Romano-Moreno et al., 2022, 2023). The mean numerical spectra are calculated from the corresponding specific spectra estimated for each random seed-based simulation.

Based on Mazzaretto et al. (2022), the root mean square error (RMSE) and bisector correlation coefficient (CORR) have been used as metrics for assessing the similarity between model- and measurement-based spectra.

$$RMSE = \sqrt{\frac{1}{n} \sum_{i=1}^{n} (x_i - y_i)^2} \tag{3}$$

$$CORR = \sqrt{\frac{\sum_{i=1}^{n} (x_i - \bar{y})^2}{\sum_{i=1}^{n} (y_i - x_i)^2 + (x_i - \bar{y})^2}} \tag{4}$$

where x_i and y_i represent the numerical and measurement spectra, S(f), through frequencies $i = 1, \ldots n$.

Joint RMSE and CORR coefficients are obtained by concatenation of the 9 frequency spectra involved per study case. CORR coefficient ranges from 0 to 1, for no correlation to total correlation, respectively. To obtain a normalized RMSE (nRMSE) value between 0 and 1, with all response variables (displacements, rotations and accelerations) equally weighted, unitary spectra (unitary area under the curve) have been considered for comparison in terms of nRMSE.

2.3.3. Historical characterization of the wave-induced response of moored ship systems at berths

From the most accurate numerical configuration previously selected, a long-term statistical characterization based on representative patterns of the multivariate response of the moored ship system to its corresponding historical climate forcing pattern-type is proposed for practical port operability assessment. This work is focused on analyzing the dynamic moored ship response induced by wave forcings. Based on Romano-Moreno et al. (2023), a multimodal harbor wave climate characterization is performed using wave agitation spectral types. The K-means algorithm (Camus et al., 2011) is applied to cluster wave agitation spectral types in a frequency-direction multivariate space, achieving a disaggregated characterization of the long-term wave agitation response at different berthing areas in a harbor, based on a reduced number of representative spectral wave agitation patterns. In this work, a further step is taken towards the characterization of the response of moored ship systems (ship motions and mooring line tensions) induced by such wave climate spectral types. In pursuit of an effective assessment, a statistical parameter-based representation is proposed for the 6-DoF moored ship motion pattern-types. The practical criteria adopted in PIANC guidelines (MarCom Working Group, 2012; working group PTC II-24, 1995) are followed in this work. That is, all six moored ship motions are characterized in terms of the significant (i.e., mean value of the highest third in each series) and maximum motion amplitude (measured from the average position in either direction; MarCom Working Group, 2012) and period parameters registered, in this case, during each event induced by the corresponding wave agitation spectral type. In addition, mooring line forces are evaluated, and the maximum load percentage of each line related to its maximum capacity (minimum breaking load, MBL), even line breakage, are also represented. In this way, a complete description of the system response, both in terms of ship motions and forces on mooring lines, is provided, which ultimately leads to a comprehensive characterization of port operability, downtime and safety at berths related to recommended operational thresholds. It should be noted that this parameter-based characterization of the moored ship system response is proposed for practical efficiency based on the standard criteria currently used. However, a detailed and readily retrievable description based on the entire time series characterization underlies this representative pattern-type definition. From such information, a thorough a characterization in terms of joint probability distributions of motion amplitude and period parameters over the event's duration is proposed. This richer characterization reveals the time variability of amplitude – period distributions during a berthing event for the different DoF and for each representative pattern-type, according to each specific mooring plan and wave climate condition. An advance from time-averaged monoparametric characterizations of moored ship motions is provided.

3. Results and discussion

In this section, the results obtained from the proposed methodology applied to the study case (the "Volcán del Teide" ferry moored at Berth 3) are presented.

3.1. Identification of the optimal numerical setup for predicting the moored ship response. Validation

First, the performance analysis of the numerical configurations defined in the catalog has been carried out for four of the monitored berthing events (A, C, D and E) in order to find the most accurate setup for predicting the moored ship response in the study case. Then, the

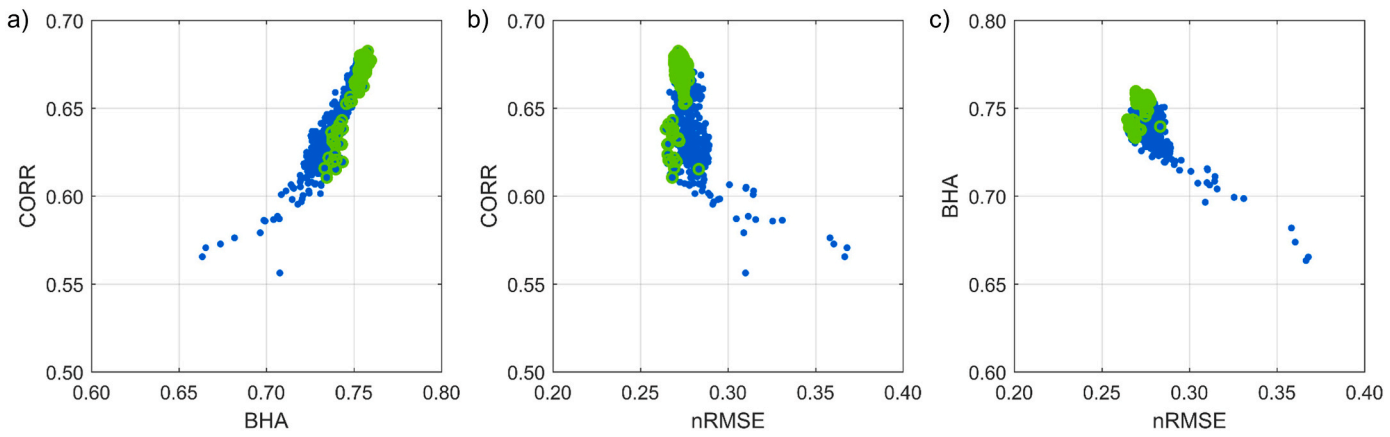

Fig. 6. Scatter plots of evaluation indexes (BHA, CORR and nRMSE) from the numerical performance analysis for the first hour of berthing event E. Visualization of the performance assessment for all the 648 numerical configurations in the catalog (blue color) and that corresponding for the 115 selected configurations in the defined sub-catalog (green color).

berthing event B has been used for validation. It has been chosen as the validation case because it presents a unique mooring plan that can be considered as an intermediate mooring arrangement between the other two available mooring plans (see Fig. 3). Berthing event E has been selected as the primary case to be numerically modeled as it also presents a unique mooring plan (Fig. 3). All 648 numerical simulations in the catalog have been performed for this event. Identifying the optimal numerical configuration in terms of the multivariate response of the moored ship is challenging for such an extensive catalog of simulations. However, from the evaluation indexes obtained for all the catalog, a subset of configurations with better quality results can be identified, while those with poorer results can be discarded. In this case, for each of the 7 h during the berthing event E, the numerical configurations providing results above the 95th percentile (the top 5% of the results) in time domain analysis have been selected, yielding a total of 115 selected numerical configurations. The results of the performance analysis for the first hour in the time length of berthing event E are presented in Fig. 6. Scatter plots of the evaluation indexes (BHA, CORR and nRMSE) for the 648 numerical configurations in the catalog are shown (blue color). Because of the high dimensionality of the results to be analyzed, Fig. 6 synthesizes all this information in a global way, showing the similarity between the multivariable numerical results and measurements, both for the time and frequency domain analyses, and for the whole catalog of simulations. Clear visualization of the predictive capability of each numerical configuration with respect to the measured data is provided. A general good agreement between the different evaluation criteria is observed. Positive correlation between BHA and CORR can be seen in Fig. 6a. Negative correlations of CORR and BHA with nRMSE can be seen in Fig. 6b and c, respectively. Additionally, the corresponding evaluation indexes for the top 115 selected configurations are shown in green. Good agreement in terms of BHA and nRMSE indexes can be seen. However, greater dispersion in terms of CORR coefficient is observed. This may be due to the different evaluation criteria, meaning that the same configurations may not be selected according to all metrics. It should be noted that the subset of 115 numerical configurations has been defined from the analysis of the results for all 7 h of the berthing event E. Therefore, the poorest indexes within this subset in Fig. 6 may correspond to numerical configurations with more accurate results for other hours of the berthing duration. These inter-hour differences of berthing event may be due to time-varying effects, such as sea level or load distribution on the ship, and to the inherent uncertainties of the numerical methodology and measurement data. For this reason, the performance evaluation considers all hours in the berthing duration.

The scatter plots in Fig. 6 show that, in general, adequate evaluation indexes are obtained for all the numerical configurations, given the complexity of the problem addressed. However, it is worth mentioning that the tail of poorest points observed in terms of the three evaluation indexes correspond to more elastic configurations, lower pretension values, and/or thinner diameters of mooring lines. On the other hand, the highest indexes are obtained for "stiffer" mooring configurations at the stern (lower elongation curve, larger line diameters, and mainly higher pretension values; see Table 4), where the aft breast line has a major influence. This could be expected since these tensioned lines restrain and hold the ship against the fenders, with the effect of friction also playing an important role in limiting horizontal motions (Rosa-Santos and Taveira-Pinto, 2013). The bounded ranges of assumed values corresponding to the 115 top simulations are summarized in Table 4 (Range $_{115}$). From the analysis of Table 4, it can be observed that more elastic mooring configurations predominate for the bow lines, mainly for the spring lines (L3 and L4), which is consistent with on-site observations of real berthing events of the study case where some of these lines appear slackened. On the other hand, stiffer mooring configurations are

Table 4
Delimitation of the assumed values for the unknown parameters. Range $_{115}$: Bounded ranges of the assumed values for the 115 top numerical configurations selected (*italics*). Opt. $_1$: Assumed values for the optimal numerical configuration selected for the study case, mooring plan "b" (non-italics).

		Diameter (mm)		Initial pretension (kN)		Load - Elongation curve		Hysteresis (%)		Z coordinate (m)	
		Range $_{115}$	Opt. $_1$	*Range $_{115}$*	Opt. $_1$	*Range $_{115}$*	Opt. $_1$	*Range $_{115}$*	Opt. $_1$	*Range $_{115}$*	Opt. $_1$
Mooring lines	**L1, L2**	*64–75*	68	*50–100*	50	*High-Low*	Low	-	–	-	–
	L3	*64–72*	68	*0–100*	0	*High-Low*	Low	-	–	-	–
	L4	*64–72*	68	*20–100*	70	*High-Low*	Low	-	–	-	–
	L5, L6	*68–75*	72	*0–100*	70	*High-Low*	Low	-	–	-	–
	L7	*68–75*	75	*100–180*	180	*High-Low*	Low	-	–	-	–
	L8	*68–75*	72	*40–120*	70	*High-Low*	Low	-	–	-	–
Fenders	**F01**	-	–	-	–	-	–	*0–20*	20	*Z*	Z
	F02, F03, F05	-	–	-	–	-	–	*0–20*	0	-	–
	F04	-	–	-	–	-	–	*0–20*	0	*Z; Z+0.5*	Z+0.5

Table 5
General characteristics of the five wave agitation spectral types selected for the analysis. Wave parameters of the three main wave components of each forcing wave agitation ST. Probability of occurrence (%). Specific selection criteria.

ST	Main wave agitation component			Secondary wave agitation component			Third wave agitation component			Prob. occ. (%)	Specific selection characteristics
	Hm_{0_1} (m)	$Tp_{\_1}$ (s)	$Dm_{\_1}$ (º)	Hm_{0_2} (m)	$Tp_{\_2}$ (s)	$Dm_{\_2}$ (º)	Hm_{0_3} (m)	$Tp_{\_3}$ (s)	$Dm_{\_3}$ (º)		
1	0.83	10.4	178	0.54	5.7	183	0.26	5.0	78	0.10	Most energetic wave agitation ST Main outer-port wave direction: NNE
2	0.24	4.6	181	0.11	10.0	176	0.09	5.0	80	26.27	Most frequent wave agitation ST Main outer-port wave direction: NNE
4	0.38	6.5	165	0.26	5.7	99	0.20	5.2	246	0.06	Main outer-port wave direction: SSE
19	0.29	16.0	176	0.10	14.6	100	0.07	3.5	178	0.91	Northern outer-port wave directions Longer outer-port wave peak period
25	0.78	17.0	176	0.33	4.9	182	0.24	15.0	98	0.004	Northern outer-port wave directions Longer outer-port wave peak period More energetic in-port wave components than ST19

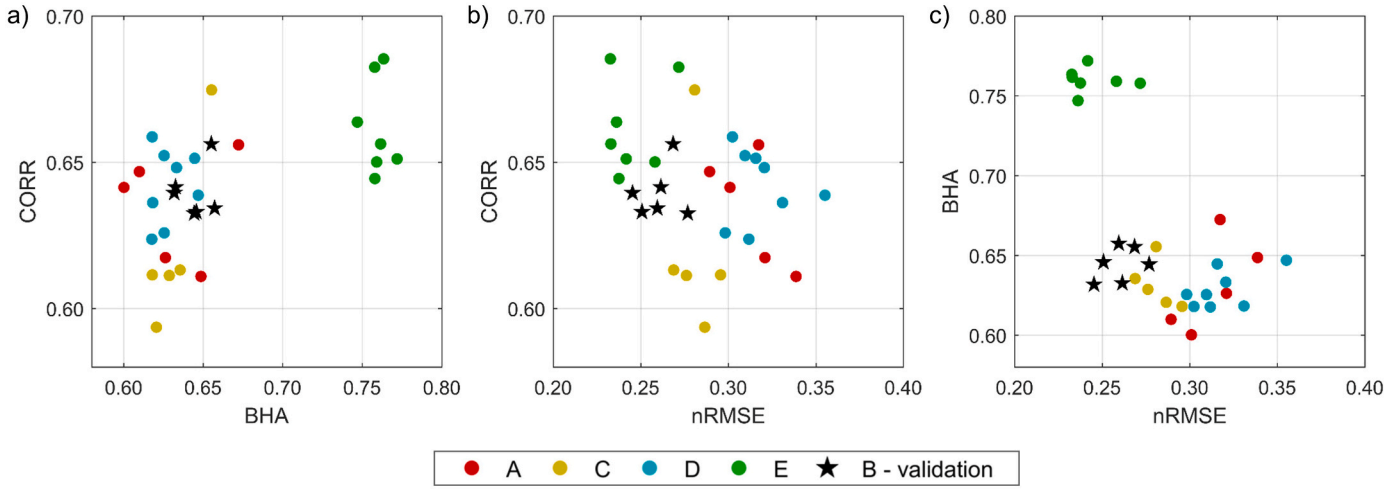

Fig. 7. Scatter plots of evaluation indexes (BHA, CORR and nRMSE) obtained for the optimal numerical configuration for all the berthing hours of events A, B, C, D and E. Visualization of the performance assessment and validation (berthing event B).

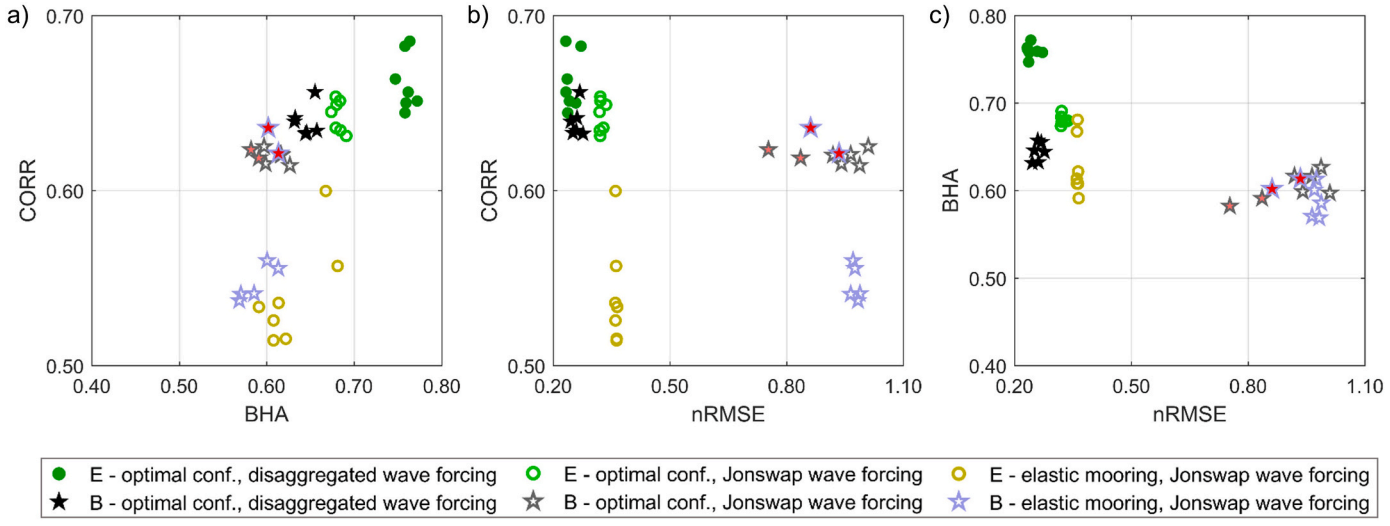

Fig. 8. Scatter plots of evaluation indexes (BHA, CORR and nRMSE) obtained for all the berthing hours of events B and E for the following comparison scenarios: 0) optimal configuration (baseline); 1) optimal numerical configuration, with the forcing spectral waves defined as a theoretical JONSWAP spectrum from the typical aggregated parameters (Hm_0, Tp, Dm, $\gamma = 3.3$ and, $\sigma_D = 20º$); 2) excessively elastic mooring configuration, with zero initial pretension and fender hysteresis values, as well as the previous JONSWAP spectrum used as forcing conditions. Visualization of the improvements achieved with the proposed methodology compared to other commonly used approaches. Red filled symbols correspond to two outstanding hours for berthing event B.

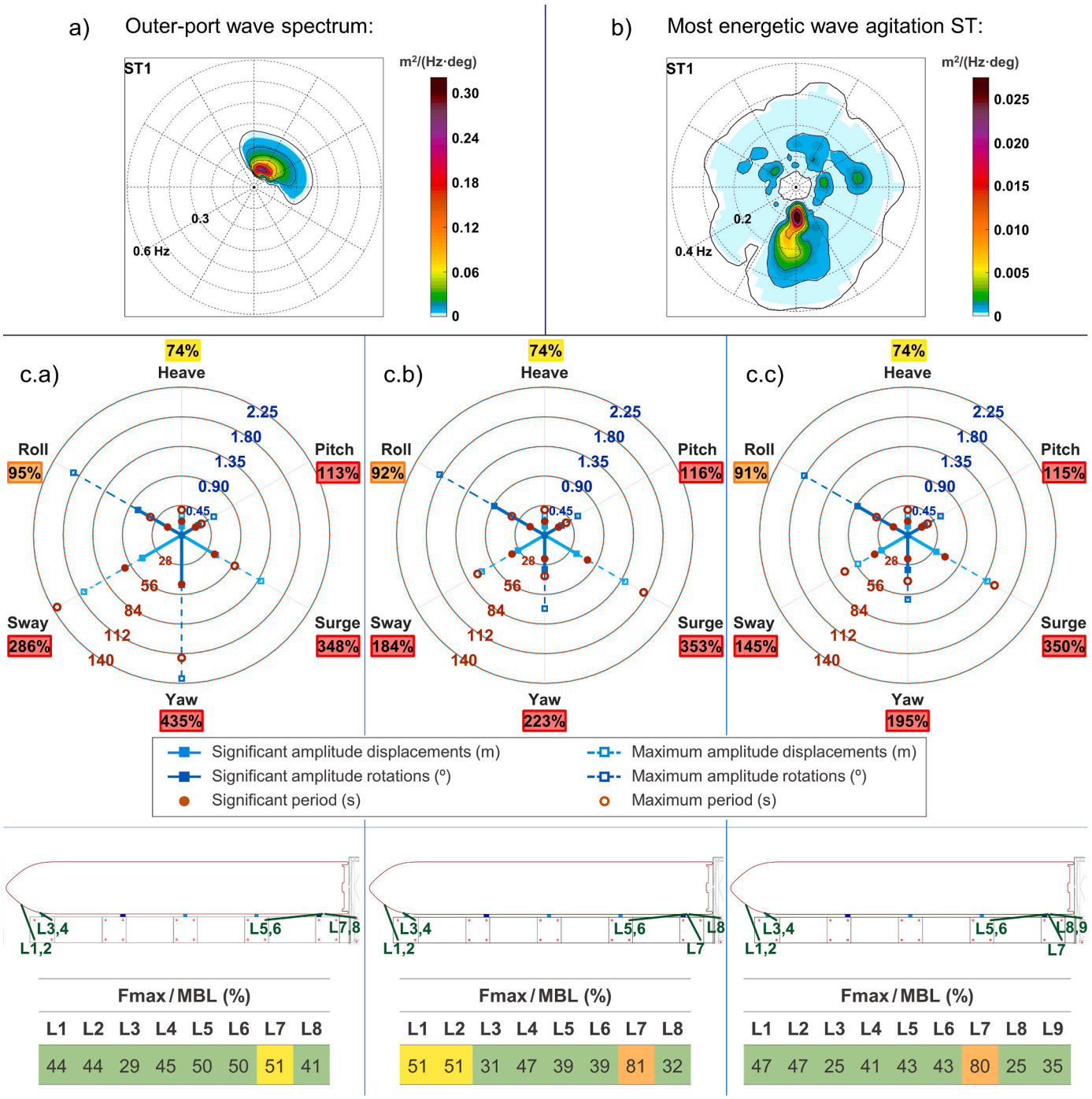

Fig. 9. Summary of the relevant information for the visualization of the multivariate dynamic response of the "Volcán del Teide" ferry forced by the most energetic wave agitation spectral type (ST1) at Berth 3. a) Outer-port wave spectrum corresponding to the wave agitation ST1 (m^2/Hz·deg); b) Wave agitation ST1 (m^2/Hz·deg); c) Representative 6-DoF moored ship motion patterns, in terms of significant and maximum motion amplitude and period values, for the three different available mooring plans from the prototype monitoring campaign (c.a, c.b and c.c); maximum load percentage (%) related to the MBL of mooring lines.

noted at the stern of the ship, mainly for the aft breast line (L7). Regarding fenders, no conclusion can be drawn at this point about the hysteresis effects, since all the assumed values are among the selected top configurations. For the Z coordinate of hanging cylindrical fenders, the value according to drawings is obtained for F01 for all cases, while variations between the initial Z and Z + 0.5 m are found for F04. This last observation about Z coordinate of F04 may comply with the actual situation, since available on-site observed information shows the F04 fender tilted in the XZ plane. Therefore, as a summary of this analysis, it can be concluded that a good first sub-catalog delimitation has been obtained to further identify the optimal configuration. To reduce the computational cost, only this subset of 115 numerical configurations has been modeled for the remaining berthing events (A, C and D). Finally, the optimal numerical setup providing the most accurate results has been identified. The corresponding assumed values for the unknown parameters are shown in Table 4 (Opt. $_1$).

As validation, the 5-h berthing event B has been modeled according to this optimal numerical configuration. The scatter plots of the evaluation indexes obtained for all the berthing events (32 berthing hours; Table 2) are represented in Fig. 7. Adequate results ($0.62 < BHA < 0.77$,

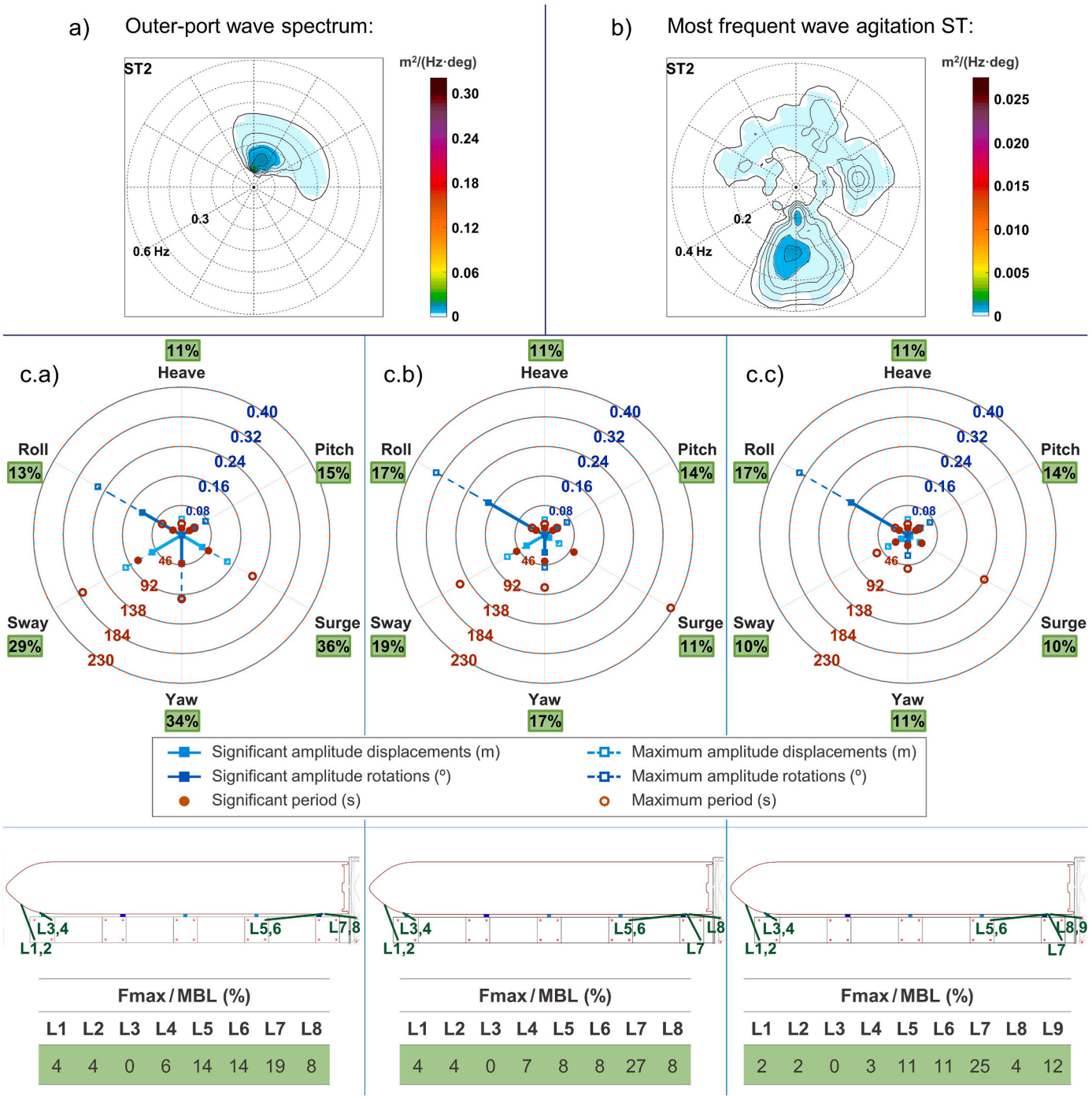

Fig. 10. Summary of the relevant information for the visualization of the multivariate dynamic response of the "Volcán del Teide" ferry forced by the most frequent wave agitation spectral type (ST2) at Berth 3. a) Outer-port wave spectrum corresponding to the wave agitation ST2 (m^2/Hz·deg); b) Wave agitation ST2 (m^2/Hz·deg); c) Representative 6-DoF moored ship motion patterns, in terms of significant and maximum motion amplitude and period values, for the three different available mooring plans from the prototype monitoring campaign (c.a, c.b and c.c); maximum load percentage (%) related to the MBL of mooring lines.

$0.59 < CORR < 0.69$, and $0.23 < nRMSE < 0.36$) are obtained for all the analyzed berthing hours. The highest accuracy is achieved for the berthing event E, especially in terms of BHA (≥ 0.75). More interspersed CORR and nRMSE results are obtained for all the berthing events. Indeed, a quite similar range of nRMSE values is obtained for the validation berthing event B ($0.25 \leq nRMSE \leq 0.28$) compared to the baseline event E ($0.23 \leq nRMSE \leq 0.27$). The good performance of the validation case (berthing event B) in terms of low nRMSE and mid-high values of BHA and CORR coefficients is worth mentioning, thus concluding the numerical configuration for predicting the multivariate response of the moored ship in the study as validated.

Another relevant issue addressed in this work for minimizing the inaccuracies introduced in the numerical predictions is the definition of an efficient coupling between the wave agitation model and the subsequent forcing of the moored ship model. The improvements achieved with the proposed methodology compared to other commonly used approaches have been quantified for berthing events E (principal case) and B (validation case), under the following two comparison scenarios: 1) optimal numerical configuration with the forcing spectral waves defined as theoretical JONSWAP spectrum from the typical aggregated

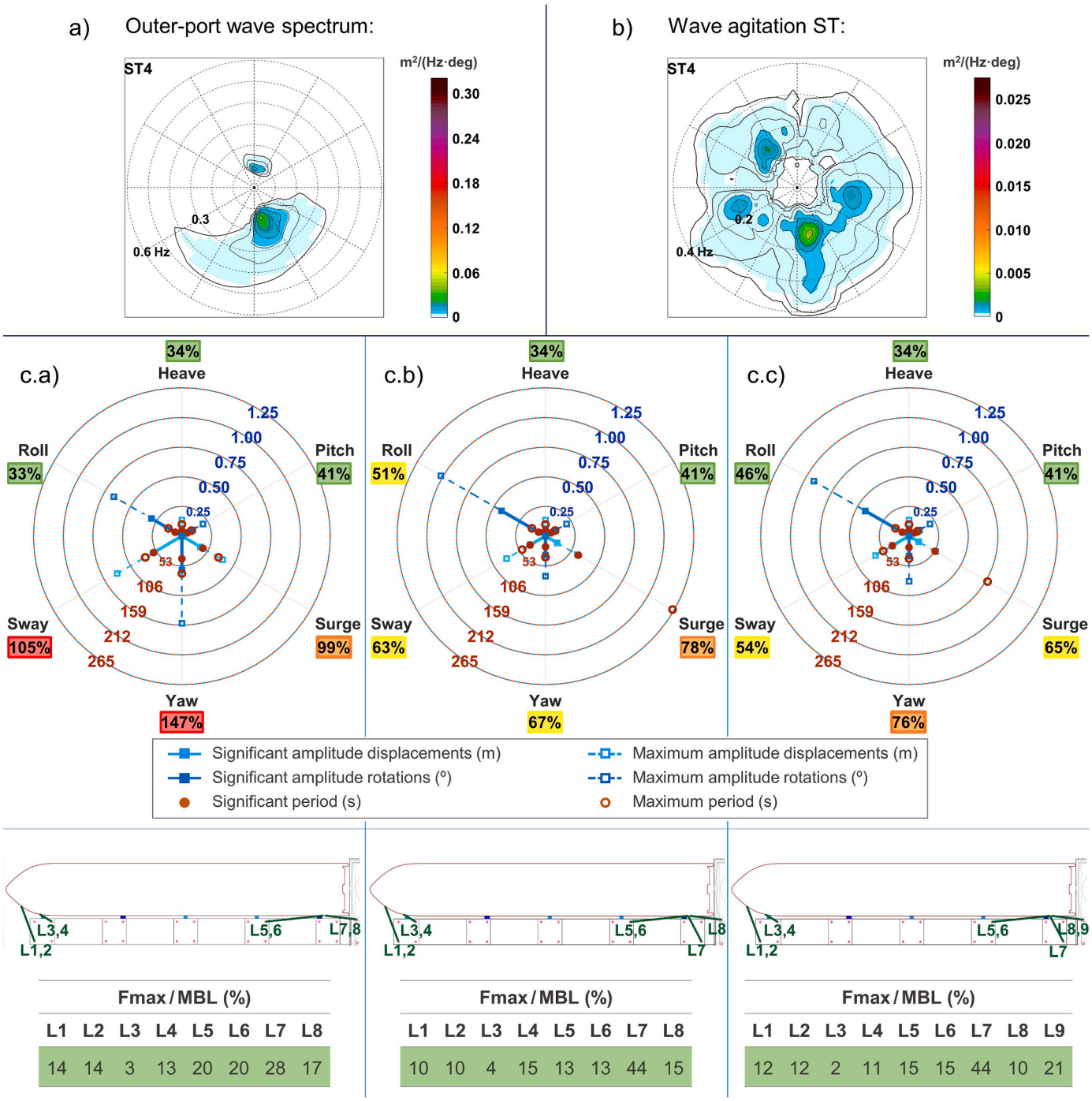

Fig. 11. Summary of the relevant information for the visualization of the multivariate dynamic response of the "Volcán del Teide" ferry forced by the wave agitation ST4 (main outer-port wave energy component from SSE) at Berth 3. a) Outer-port wave spectrum corresponding to the wave agitation ST4 (m^2/Hz·deg); b) Wave agitation ST4 (m^2/Hz·deg); c) Representative 6-DoF moored ship motion patterns, in terms of significant and maximum motion amplitude and period values, for the three different available mooring plans from the prototype monitoring campaign (c.a, c.b and c.c); maximum load percentage (%) related to the MBL of mooring lines.

parameters (Hm_0, Tp, Dm, peak enhancement factor, $\gamma = 3.3$ and gaussian directional spreading, $\sigma_D = 20°$); 2) excessively elastic mooring configuration with zero pretension and hysteresis, forced with the previous JONSWAP spectrum. The comparison results are presented in Fig. 8, where the poorer quality (error increases of more than 250%) of the moored ship response predictions obtained when using theoretical unimodal definitions and standard parameterizations of the spectral wave forcing conditions can be observed. The worst overall results are observed for scenario 2 (excessively elastic mooring configuration, JONSWAP forcing spectrum). However, 2 h of event B stand out (red filled symbols in Fig. 8), in which its prediction, in terms of BHA and CORR (not so in nRMSE), is better than that from scenario 1. At this point, three main aspects should be pointed out. First, these results suggest that more deviated-from-actual numerical configurations could be selected as optimal due to the less accurate and commonly used definitions of the wave forcings. Second, the evaluation obtained with the different metrics demonstrates the importance of multivariate analysis in both the time and frequency domains. Third, the limitations

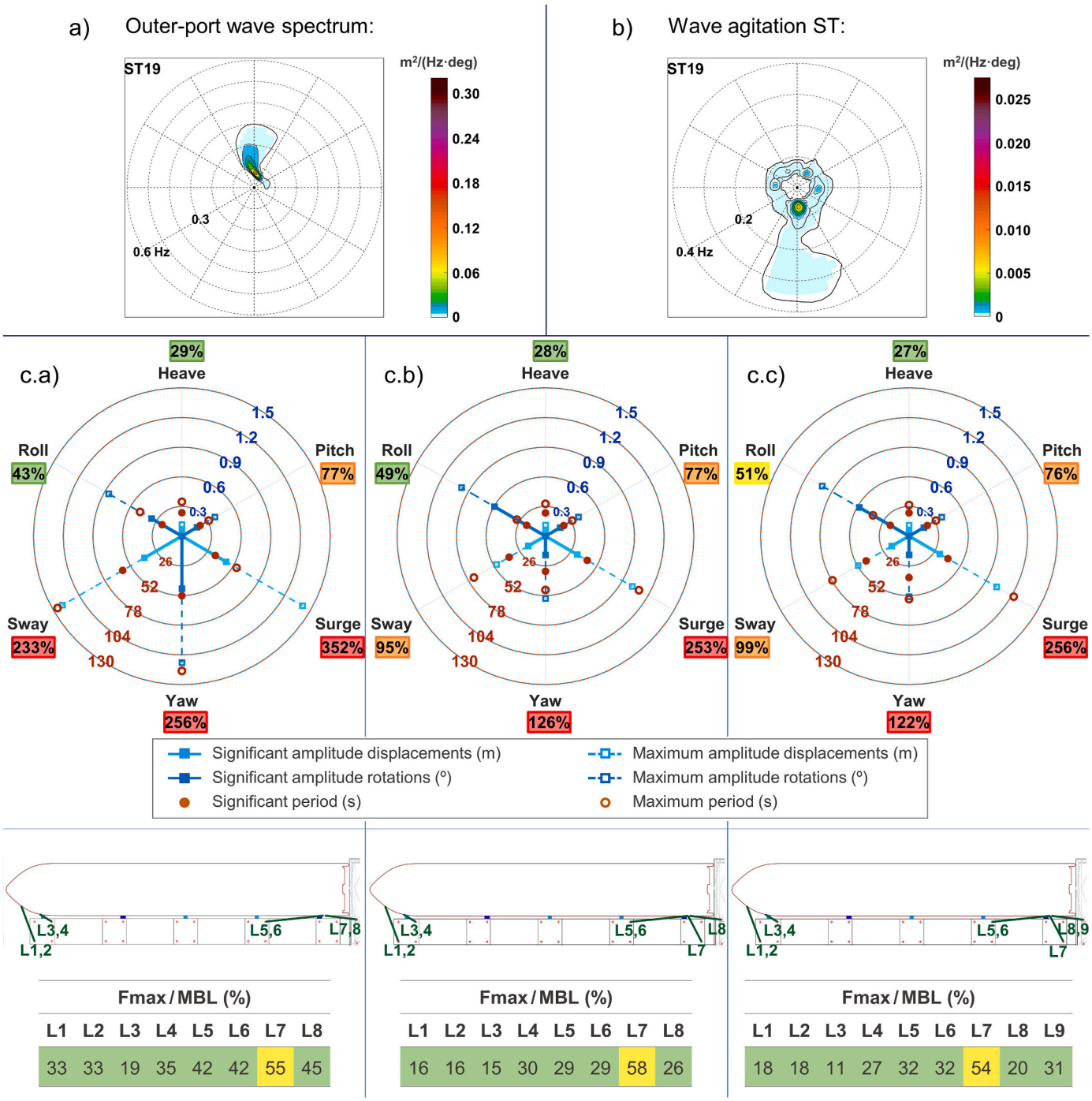

Fig. 12. Summary of the relevant information for the visualization of the multivariate dynamic response of the "Volcán del Teide" ferry forced by the wave agitation ST19 (main outer-port wave energy component from N with longer Tp) at Berth 3. a) Outer-port wave spectrum corresponding to the wave agitation ST19 (m^2/Hz·deg); b) Wave agitation ST19 (m^2/Hz·deg); c) Representative 6-DoF moored ship motion patterns, in terms of significant and maximum motion amplitude and period values, for the three different available mooring plans from the prototype monitoring campaign (c.a, c.b and c.c); maximum load percentage (%) related to the MBL of mooring lines. Relative percentage to the recommended operational thresholds (or MBL for mooring lines) is indicated by the color scale (in increasing order: green, 0–50%; yellow, 51–75%; orange, 76–99%; red, ≥100%).

of single event-based approaches are shown by this last observation, where general misleading conclusions could be drawn from only considering those isolated deviant results.

3.2. *Long-term statistical characterization of wave-induced response of moored ship systems at berths*

This last step involves the historical characterization of the multivariate response of the "Volcán del Teide" ferry moored at Berth 3 using the validated numerical setup. As part of a comparative analysis to provide a practical mooring optimization assessment, the response of the study moored ship has been evaluated for the three different actual mooring plans available from the prototype monitoring campaign (Fig. 3). First, a multimodal wave agitation climate characterization based on 5 × 5 frequency-direction wave agitation spectral types was carried out at Berth 3, according to Romano-Moreno et al. (2023). Five

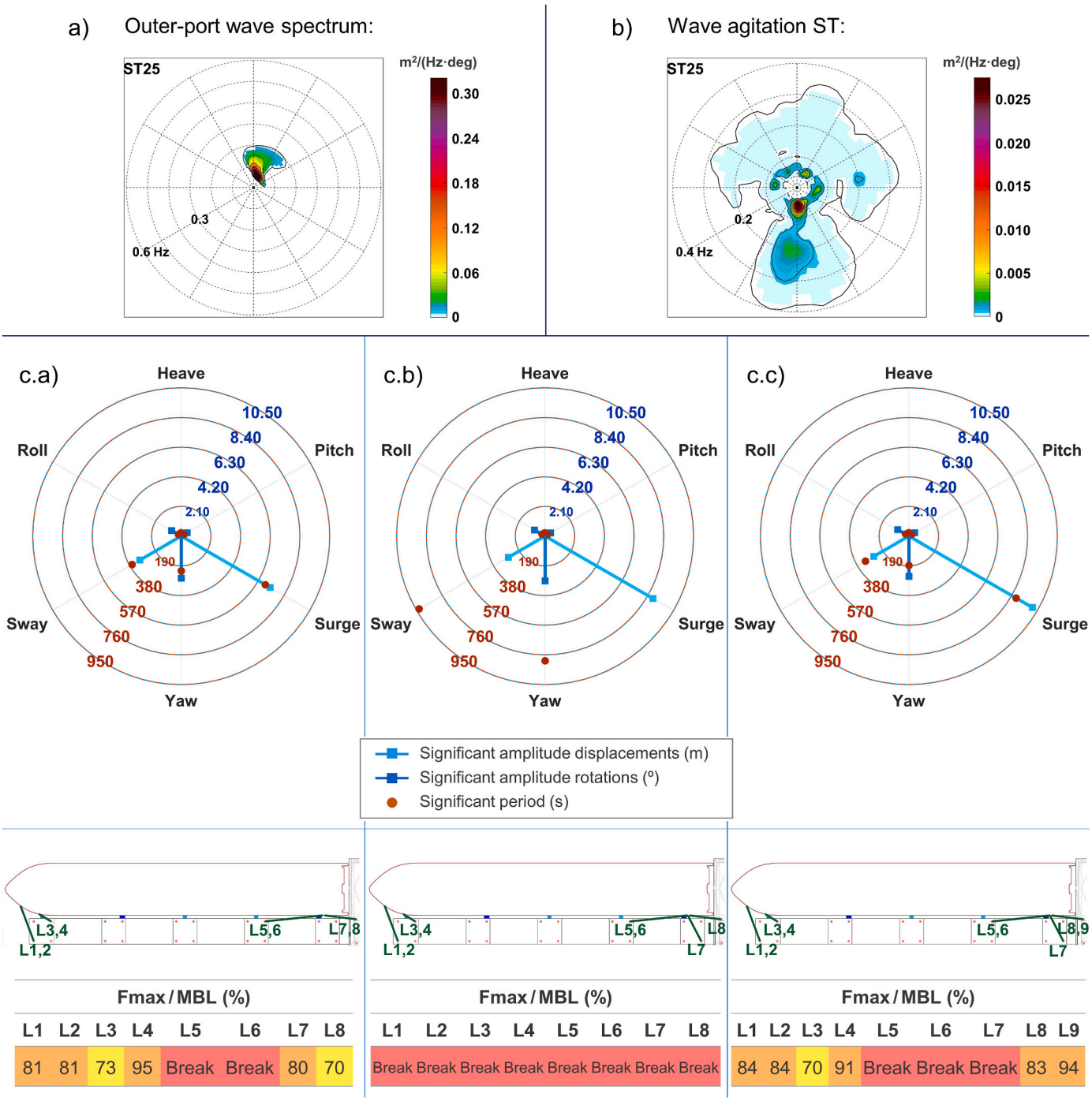

Fig. 13. Summary of the relevant information for the visualization of the multivariate dynamic response of the "Volcán del Teide" ferry forced by the wave agitation ST25 (main outer-port wave energy component from N with longer Tp) at Berth 3. a) Outer-port wave spectrum corresponding to the wave agitation ST25 (m^2/Hz·deg); b) Wave agitation ST25 (m^2/Hz·deg); c) Representative 6-DoF moored ship motion patterns, in terms of significant motion amplitude and period values, for the three different available mooring plans from the prototype monitoring campaign (c.a, c.b and c.c); maximum load percentage (%) related to the MBL of mooring lines. Relative percentage to the recommended operational thresholds (or MBL for mooring lines) is indicated by the color scale (in increasing order: green, 0–50%; yellow, 51–75%; orange, 76–99%; red, ≥100%).

different wave agitation spectral types (ST1, ST2, ST4, ST19 and ST25) were selected as relevant sea states for the current analysis. Their main characteristics are summarized in Table 5.

Secondly, the response of the moored ship systems induced by each forcing wave agitation ST has been numerically modeled following the approach described in Section 2.3.1. This involved 3-h simulations, 3 random start seeds for irregular wave signal generation and 0.2 s time step. Since this historical characterization is focused on the wave-induced response of the study moored ship system at berth, numerical simulations with no forcing wind have been performed. A mean sea water level of 1.5 m (maximum tidal range of 3 m in the study area, Section 2.1) has been defined for all numerical runs. Third, the proposed definition of the representative patterns of the multivariate response of the moored ship system is represented in terms of ship motion amplitude and period parameters, including the relative percentage to the recommended operational thresholds, and the maximum load percentage

related to the MBL of mooring lines. The following operational thresholds, in terms of maximum motion amplitudes, have been considered, respectively for surge, sway, heave, roll, pitch and yaw: 0.4 m, 0.6 m, 0.4 m, 2.0º, 0.5º and 0.5º. It should be noted that these values have been defined according to the maximum motion range-based criteria recommended in PIANC 1995 (working group PTC II-24, 1995) for ferries/ro-ro ships, converted to maximum motion amplitudes for consistency with the practical criteria adopted according to PIANC 2012 (MarCom Working Group, 2012). The results are represented in Figs. 9–13. The relevant forcing outer- and in-port wave spectral types are shown in panels a) and b), respectively. The representative 6-DoF moored ship motion patterns, in terms of significant and maximum motion amplitude and period values, are presented in panels c.a), c.b) and c.c), respectively, for the three different available mooring plans from the prototype monitoring campaign. It consists of a 6-axis graph, where each axis represents a mode (DoF) of ship motion. The axis magnitude is indicated in circular form, with different colors for amplitude and period parameters. The operability level associated with each response variable is represented by a color scale indicating the relative percentage of the maximum motion amplitudes to the recommended operational thresholds, as follows: green $\leq$ 50%; yellow = 51–75%; orange = 76–99%; red $\geq$ 100% = threshold exceedance. Finally, the maximum load percentage (%) related to the MBL of mooring lines is also indicated adopting the same color scale. From the analysis of these results, a multi-process and multi-variable assessment of port operability at berths is provided based on the final response of each moored ship system related to both the historical outer- and in-port spectral wave climate conditions. First, the analysis information for the most energetic (ST1) and most frequent (ST2) wave agitation spectral types is summarized in Figs. 9 and 10, respectively. As described in Section 2.2, the predominant wave climate conditions in the vicinity of the Africa basin are coming from NNE wave directions, with Tp between 5 and 15 s (Fig. 9a and 10a). These waves impact on the study Berth 3 as the main in-port wave energy components coming from southern directions (Fig. 9b and 10b). The system response patterns for the three mooring plans are presented in Fig. 9c and 10c (c.a, c.b and c.c, respectively, for mooring plans “a”, “b” and “c” in Fig. 3). As expected, noticeable higher motion amplitudes are observed for the most energetic forcing wave agitation spectral type (ST1, Fig. 9). The largest significant motion amplitudes are observed for the mooring plan “a” (Fig. 9c a), specifically, for sway (A_S = 0.69 m) displacement, and roll (A_S = 0.77º) and, slightly lower, yaw (A_S = 0.75º) rotations. For mooring plans “b” and “c”, with the pretensioned aft breast line (L7; Fig. 9c b and c.c), sway and yaw motions are considerably reduced, especially for mooring plan “c” (significant and maximum value reduction over 30% and 50%, respectively) with an additional stern line (L9; Fig. 9c c). Surge, heave, roll and pitch motions remain similar and, mostly, the high load percentage (around 80%) on line L7 is worth mentioning. Motion periods in the range of those of forcing waves are observed for heave, roll and pitch motions. Noticeable longer periods are observed for surge, sway and yaw. In terms of operability level according to parameterized-based practical criteria, for the three mooring plans, the maximum allowable amplitudes are exceeded for surge, sway, pitch and yaw motions, while roll is almost reaching it, and heave remains below 75%.

Similar patterns are observed in Fig. 10, albeit with much smaller values of ship motion amplitudes and forces on mooring lines, for the most frequent forcing wave agitation spectral type (ST2). The highest significant amplitudes are obtained for sway motion with mooring plan “a” (Fig. 10c a) and for roll motion with mooring plans “b” and “c” (Fig. 10c b and c.c). Fully operational results are obtained for this wave agitation ST2, which is the most frequent ST at Berth 3.

Secondly, as described in Section 2.2, less probable outer-harbor waves with main wave directions from SE-SSE and Tp between 5.0 and 7.5 s, such as the wave spectrum shown in Fig. 11a, are also present in the vicinity of the study port basin. These wave conditions directly impact on the study Berth 3 with incoming wave energy components from SSE directions, as well as reflected waves from western inner port contours (Fig. 11b). In this case, sway and roll DoF present the highest significant amplitude values for the three mooring plans (up to A_S = 0.28 m for sway in mooring plan “a”; and roll A_S = 0.43º for mooring plan “b”). The relatively high A_S (0.28º) of yaw for the mooring plan “a” (Fig. 11c a) should also be noted, exceeding the recommended operational threshold. Again, important reduction of significant amplitude values (between 36% and 48%) for surge, sway and yaw moored ship motions can be observed for mooring plans “b” and “c” compared to mooring plan “a”. Indeed, inoperative values of sway and yaw for mooring plan “a”, become operational values for mooring plans “b” and “c” (Fig. 11c). Higher operability levels relative to surge motion are also obtained for mooring plans “b” and mainly “c”. Increased roll amplitude values are observed, but they remain operative for all mooring plans. Low tension rates ($\leq$ 44%) are observed for all mooring lines. In conclusion, this global vision provided of the operational landscape brings relevant information towards maximizing operability at the berths, for example for the ship’s personnel or operators to define the appropriate mooring plan in the study case according to the met-ocean conditions or forecasts.

Third, the response of the moored ship system induced by wave agitation spectral types, which in turn are forced by outer-port main wave energy components coming from northern directions with longer Tp around 16–17 s (ST19 and ST25; Figs. 12 and 13), is analyzed. Characteristic wave agitation patterns arise at Berth 3, with most of the wave energy contained in a peaked main wave component with such longer Tp and strongly southern direction, i.e., the main forcing wave conditions acting longitudinally on the moored ship. Therefore, the surge mode is the main induced displacement of the moored ship forced by wave agitation ST19 (surge A_S = 0.52 m, 0.37 m and 0.36 m, for mooring plans “a”, “b” and “c”; Fig. 12). The large sway and yaw amplitudes for mooring plan “a” should be noted. Significant amplitude reductions of up to 30% in surge, 55% in sway and 64% in yaw are obtained for mooring plans “b” and “c” compared to plan “a”. However, these motion amplitude reductions are not enough to meet the recommended operational criteria for yaw and, especially, surge motions for any of the three mooring plans.

In terms of total wave agitation, this ST19 presents a total wave height at Berth 3 similar to that from ST2 (around 0.3 m), and lower than that of the previous ST4 (0.5 m). However, much worse operability levels, in fact, highly inoperative levels result from ST19. It is also worth noting that the value of total Hm_0 = 0.3 m is quite below the operational threshold of 0.5 m defined in Thoresen (2003) and ROM 3.1–99 (for longitudinal actions to the quay such as the current one; Puertos del Estado, 1999). This results demonstrates the importance of properly characterizing all the processes involved. In this work, the complete characterization of the local wave conditions at Berth 3, based on the frequency-direction wave energy distribution is used, going beyond the typical aggregated parameters. Furthermore, the proposed multi-process and multi-variable assessment of port operability/downtime provides a comprehensive characterization allowing to identify specific problematic wave climate and mooring conditions even though in terms of usual criteria they do not appear to be unfavorable conditions. This point is further supported, not only in terms of operability but also in terms of safety, by the following ST25 (Fig. 13), which presents a more energetic and shape-similar waveform to the ST19. In terms of wave agitation, ST1 is the most energetic wave agitation pattern. However, the following results show that ST25 is significantly more problematic for port operability and safety. As shown in Fig. 13c, mooring line breakage occurs for all three considered mooring plans. For this reason, only the significant parameters are presented in the representative 6-DoF moored ship motion patterns. Since upon line breakage, the maximum values resulting from the numerical model become excessive due to the large motions of the ship moving away from the berth. The significant surge period for mooring plan “b” (Fig. 13c b) is also not represented because it is far out of the

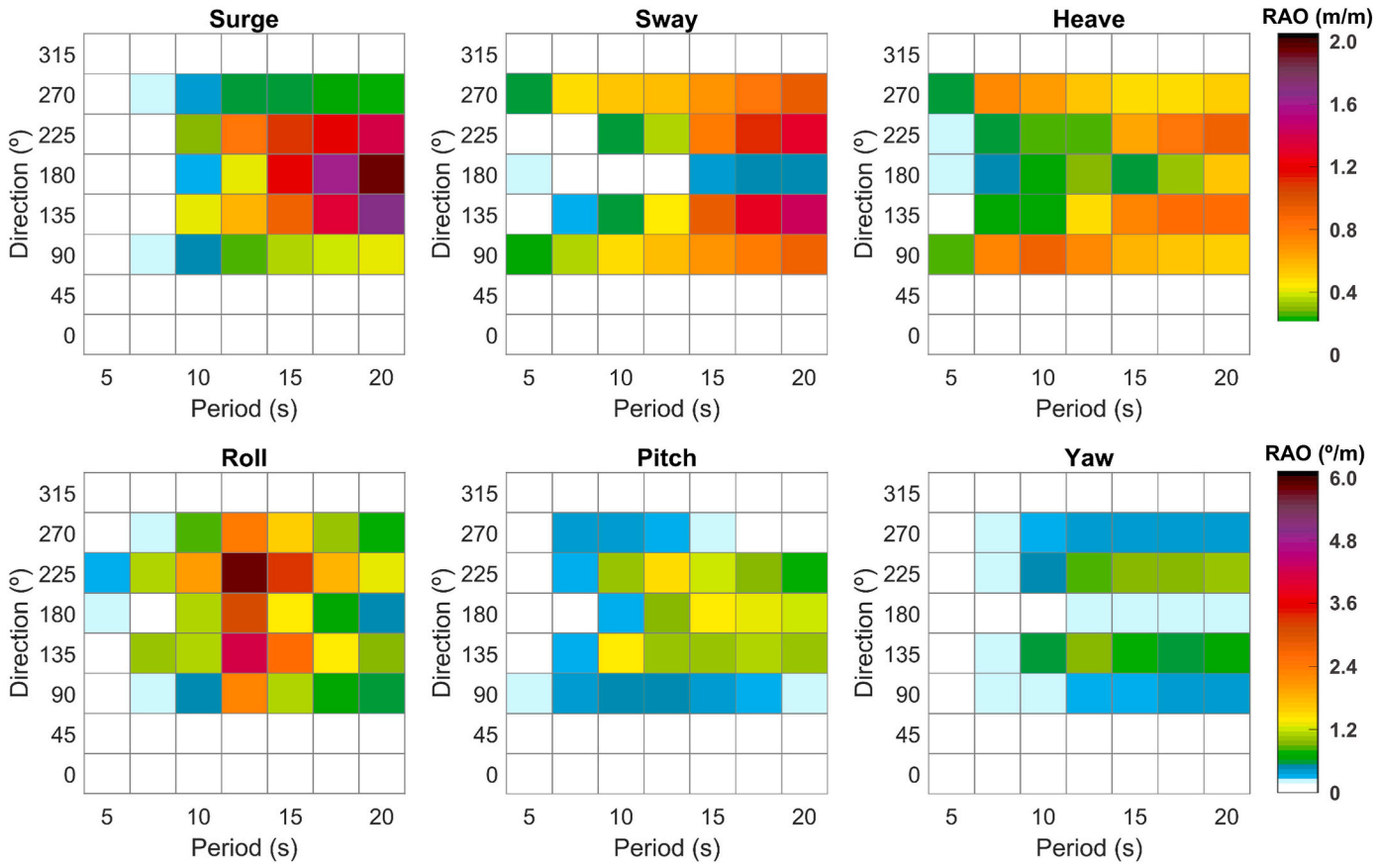

Fig. 14. Response Amplitude Operator (RAO). Visualization of the wave-induced response of the study free-floating ship, in terms of motion/height of incident regular waves ratio, for each DoF, in a wave Period (s) – wave Direction (°) space. Only the response to linear wave forces is represented.

limits shown. Therefore, since the maximum amplitude values are not considered, the comparison with respect to the recommended thresholds cannot be quantified either, nor would it be meaningful since line breakage already represents a serious exceedance of those operational and safety limits. From the analysis of motion patterns in Fig. 13, the exceedingly high values of significant motion amplitudes of sway, yaw and, especially, surge, resulting from line breakage can be observed. Furthermore, although not shown here for brevity, other mooring plans (with different mooring arrangements and initial pretension values) have also been analyzed for this forcing wave agitation ST25, and mooring line breakage has been obtained for all of them. As a result, downtime and non-staying ship events may be expected for the study ferry at Berth 3 for these wave climate conditions.

This extreme behavior can be explained by the Response Amplitude Operator (RAO) representation in Fig. 14, which shows the ship response induced by 1-m (height) regular waves with different period and direction is represented for each DoF. It should be noted that only the response to linear wave forces is represented (Arcadis, 2016a). The range of incident wave directions between 90 and 270° has been considered in computations due to the orientation of the study Berth 3 (Fig. 1b and 4a). The considered range of wave periods is 5–20 s. As shown, the highest ship response amplitudes are obtained for the following wave period (T) – direction (D) pairs, respectively, for each DoF: T = 20 s – D = 180° for surge; T = 20 s – D = 135° for sway; T = 20 s – D = 225° for heave; T = 12.5 s – D = 225° for roll and pitch; T = 20 s – D = 225° for yaw. Therefore, the highest RAO values for surge, sway, heave and yaw motions are mainly shown for longer incident wave periods (15–20 s), and wave directions between 135 and 225°, which correspond to the main in-port wave energy components in the wave agitation ST19 and ST25. As mooring lines are primarily used to restrain the moored ship mainly against the horizontal motions (i.e., surge, sway and yaw), these RAO results are consistent with the higher relative magnitude of such motions observed for the forcing wave agitation ST19 (Fig. 12c), compared to the previously analyzed STs (ST1, ST2 and ST4 in Figs. 9–11, respectively), and especially with the mooring line breakage events identified for the more energetic ST25 (Fig. 13).

Finally, it should be noted that the representative pattern-type definition has been proposed for the sake of effective and practical assessment of port operability according to standard criteria commonly used. Taking a step beyond these parametric approaches, an advanced characterization is proposed, as a complement to the previous one, based on joint probability functions of amplitudes ($A_{Z\text{-}P}$) and periods ($T_{Z\text{-}Z}$) calculated from the entire time series of motions for each representative berthing event (each forcing wave agitation ST and mooring plan). This characterization based on joint amplitude – period distributions has been performed for all the representative berthing events. However, to abbreviate the analysis in this work, only some relevant results showing the improvements achieved are presented below.

For example, Figs. 15 and 16 show the $A_{Z\text{-}P}$ – $T_{Z\text{-}Z}$ joint probability distributions for the "Volcán del Teide" ferry at Berth 3 with mooring plans "a" and "b" for the most energetic wave agitation ST1 (Fig. 9). The significant and maximum amplitude and period values previously presented in the corresponding representative pattern-types are also indicated by the black dots and unfilled black circles, respectively, as well as the recommended operational thresholds of maximum motion amplitudes are shown by red lines. The general reduction of motion amplitudes (mainly horizontal motions) when adding the aft breast line can be observed for plan "b" compared to plan "a". The slight increase in roll motion can also be seen. According to the recommended parametric thresholds, both are notably inoperative (downtime) related to surge, sway, pitch and yaw (see Fig. 9). However, quite different $A_{Z\text{-}P}$ – $T_{Z\text{-}Z}$ distributions can be observed in Figs. 15 and 16, with most of the

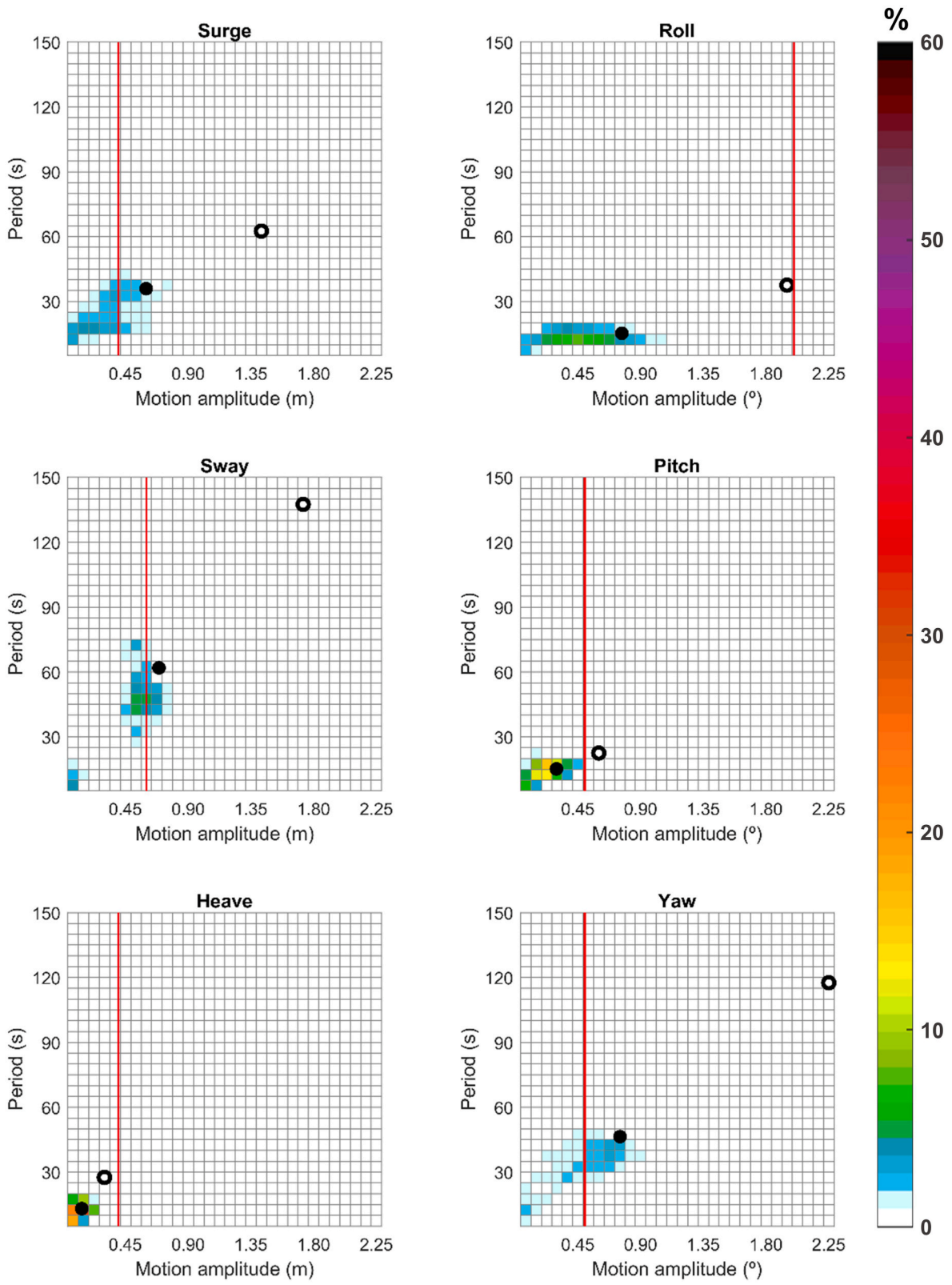

Fig. 15. 6-DoF joint probability functions of moored ship motion $A_{Z\text{-}P}$ and $T_{Z\text{-}Z}$ calculated from resulting numerical time series of motions; forcing wave agitation ST1; mooring plan "a". Significant (black dots) and maximum (unfilled black circles) amplitude and period parameters. Recommended operational thresholds of maximum motion amplitudes according to PIANC standards (working group PTC II-24, 1995; MarCom Working Group, 2012) (red lines).

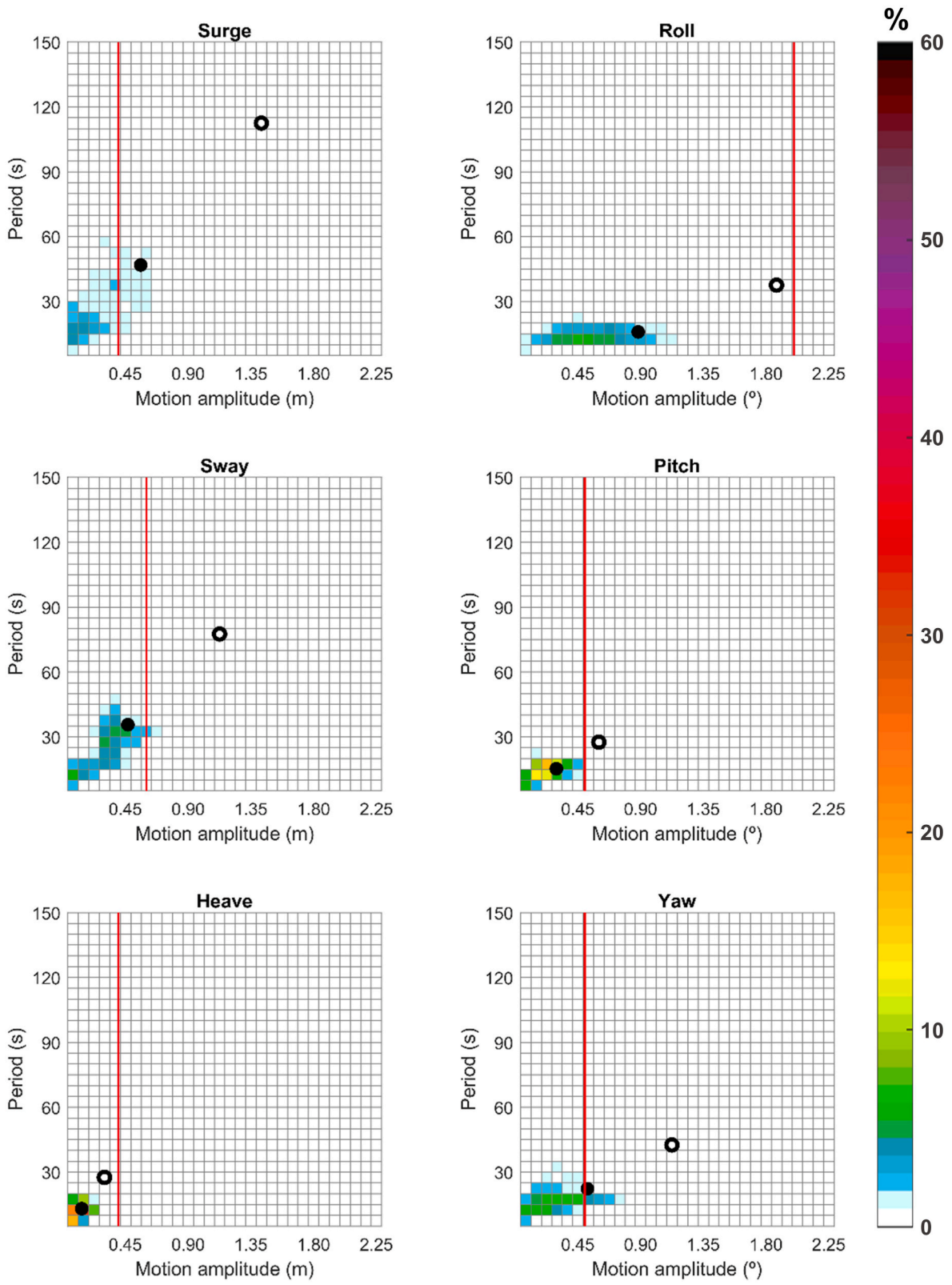

Fig. 16. 6-DoF joint probability functions of moored ship motion $A_{Z\text{-}P}$ and $T_{Z\text{-}Z}$ calculated from resulting numerical time series of motions; forcing wave agitation ST1; mooring plan "b". Significant (black dots) and maximum (unfilled black circles) amplitude and period parameters. Recommended operational thresholds of maximum motion amplitudes according to PIANC standards (working group PTC II-24, 1995; MarCom Working Group, 2012) (red lines).

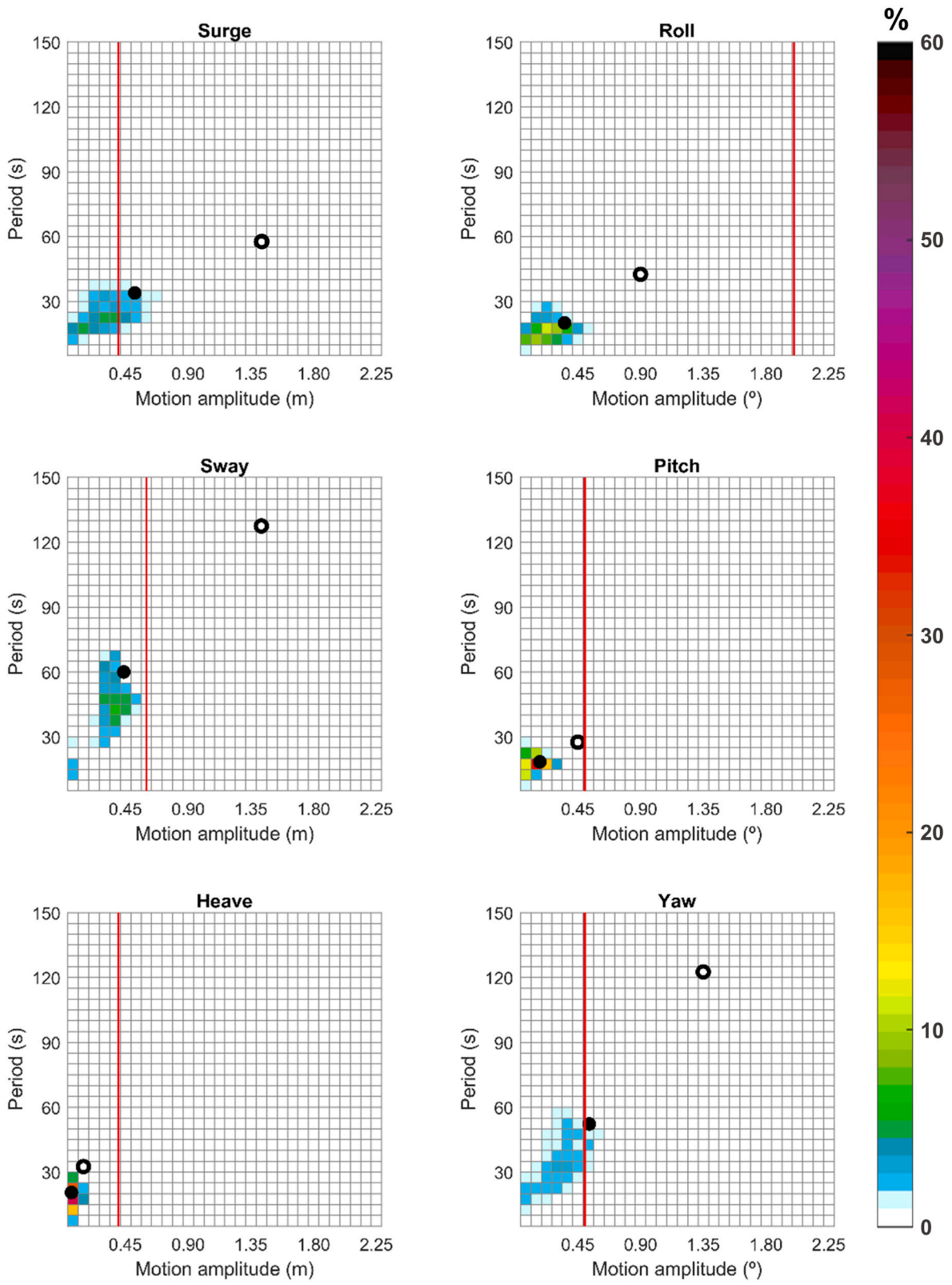

Fig. 17. 6-DoF joint probability functions of moored ship motion $A_{Z\text{-}P}$ and $T_{Z\text{-}Z}$ calculated from resulting numerical time series of motions; forcing wave agitation ST19; mooring plan "a". Significant (black dots) and maximum (unfilled black circles) amplitude and period parameters. Recommended operational thresholds of maximum motion amplitudes according to PIANC standards (working group PTC II-24, 1995; MarCom Working Group, 2012) (red lines).

distribution below the recommended operational limit for mooring plan "b". Therefore, a considerably better port operability might be expected for this mooring scenario, despite showing some similar single-value parameters, such as those of surge. This leads to an interesting thought-provoking point about the representativeness of parameterized operational threshold definitions.

The obtained results for the forcing wave agitation ST19 (Fig. 12) and mooring plan "a" are shown in Fig. 17. Lower amplitudes and longer periods, predominantly between 15 and 25 s and coinciding with wave periods, can be seen for heave, pitch and roll motions, which are most directly related to waves. Considerably more similar shape distributions to those in Fig. 15 (for ST1, mooring plan "a"), although narrower in smaller amplitude values, can be observed for horizontal motions, especially sway and yaw (Fig. 12). Slightly more concentrated distribution, even in a narrower range of periods, can also be observed for surge motion. This is consistent with the lower significant amplitude and period values of surge motion obtained for ST19 compared to those for ST1. However, the slightly higher maximum surge amplitude is worth mentioning, leading to greater downtime. This analysis demonstrates the complex variability of the underlying physics of each response variable.

To conclude, this further characterization reflects the time variability of the multivariate response of moored ship over the representative berthing events' duration, which can represent an important advance from the time-averaged parametric approaches for increased-accuracy port operability assessment and optimization.

4. Conclusions

A novel methodology for multi-process and multi-variable assessment of port operability/downtime in harbors, based on the historical characterization of the gravity wave-induced response of moored ship systems at berths, in relation to both the historical outer- and in-port spectral wave climate, has been presented in this paper. The complete methodology has been described, applied and validated with prototype measured data for a real berthing scenario in Las Palmas Port (Spain).

A joint numerical modeling and statistical analysis has been adopted. First, a numerical optimization approach is presented seeking to minimize the significant uncertainty levels that are often associated with numerical modeling/predictions of moored ship response due to the unavailability of important information required for proper model configuration (mooring and fendering system) and forcing. Advantage is taken of the available information from a monitoring campaign for the challenging task of identifying the optimal numerical configuration for predicting the multivariate response of the moored ship from an extensive catalog. A multivariate performance evaluation, in both time and frequency domain, has been performed based on the complete time and spectral distributions of each response variable, rather than the classical time-averaged or spectrum-aggregated parameterizations of moored ship motions. This analysis has allowed the determination of an appropriate numerical setup providing adequate and consistent predictions with the expected (on-site observations), and quantifying the level of accuracy achieved. In addition, an efficient coupling between the wave agitation/harbor tranquility model and the subsequent forcing of the moored ship model has been adopted. The improvements achieved with the proposed methodology compared to other commonly used approaches, such as theoretical unimodal definitions and standard parameterizations of the spectral wave forcing conditions, single-event based approaches, or non-optimal mooring/fendering configurations assumed, have been quantitatively demonstrated.

From the final numerical setup selected, progress has been made for a comprehensive, long-term statistical assessment of port operability at berths. A characterization based on representative patterns of the multivariate response of the moored ship system, including ship motions and mooring line tensions, to its corresponding historical climate forcing pattern-types is proposed for practical assessment of port operability/downtime and even safety at berths related to recommended operational thresholds. An efficient interpretation of the main processes involved, even for different scenarios (such as mooring plans in this work), and a direct relationship with the multi-variable operability levels in a single and global visualization. This has been proven to be a relevant aspect, providing relevant information towards maximizing operability at the berths, for example for the ship's personnel or operators to define the appropriate mooring plan in the study case according to the met-ocean conditions or forecasts. In addition, the importance of properly characterizing all the processes involved has been demonstrated by the proposed multi-process characterization allowing to identify specific problematic wave climate and mooring conditions even though in terms of usual criteria (e.g., in-port wave agitation/harbor tranquility, total wave height) they do not appear to be unfavorable conditions for port operability and safety. Finally, a step forward has been taken from parameter-based approaches towards a thorough characterization in terms of joint motion amplitude – period distributions, representing the time variability of motions during each representative berthing event. An advance from time-averaged monoparametric characterizations of moored ship motions is provided for increased-accuracy port operability assessment and optimization. An interesting thought-provoking point about the representativeness of parameterized operational threshold definitions arise, as inoperative conditions according to the maximum amplitude thresholds have been found presenting probability distributions mostly below the recommended limits.

To conclude, the improvements achieved with the proposed methodology may lead to enhanced assessment and/or prediction of port operability/downtime levels and safety at berths, both for historical characterization, nowcasting, and future planning, management and forecasting.

Additionally, it is worth mentioning that short (gravity) waves, with typical wave periods between 3 and 30 s, are the only wave forcing considered in this work for the analysis of the wave-induced response of moored ships at berths. However, infragravity waves (bound and free long waves, with wave periods typically between 30 and 600 s) can also have major impacts on the performance of port operations in some harbor basins, especially due to resonant amplification effects. This important infragravity-resonance phenomenon forcing the moored ship response is contemplated in a future research of the authors, extending the current methodology.

Credit author statement

Eva Romano-Moreno: Conceptualization, Methodology, Investigation, Data curation, Resources, Formal analysis, Writing – original draft preparation. **Gabriel Diaz-Hernandez**: Conceptualization, Methodology, Investigation, Resources, Supervision, Funding acquisition, Writing – Critical review. **Antonio Tomás**: Conceptualization, Methodology, Investigation, Resources, Funding acquisition, Writing – Critical review. **Javier L. Lara**: Investigation, Supervision, Funding acquisition, Writing – Critical review.

Declaration of competing interest

The authors declare that they have no known competing financial interests or personal relationships that could have appeared to influence the work reported in this paper.

Data availability

No data was used for the research described in the article.

Acknowledgments

The authors would like to thank the Port Authority of Las Palmas and Naviera Armas shipping company for their cooperation and the

information provided; CEHINAV-UPM Research Group (ETSI de Caminos, Canales y Puertos, Universidad Politécnica de Madrid) for assistance in the interpretation of instrumental data from the prototype monitoring campaign; Trama Ingenieros for the collaboration and support during the field campaign and collection of information; and Arcadis for the SHIP-MOORINGS model license.

This work was supported by a FPU (Formación de Profesorado Universitario) grant from the Spanish Ministry of Science, Innovation and Universities to the first author (FPU18/03046). The authors acknowledge the financial support from the Government of Cantabria through the Fénix Programme. This work was also partially funded under the State R&D Program Oriented to the Challenges of the Society (PID2020-118285RB-I00) of the Spanish Ministry of Science, Innovation and Universities.

References

Abdelwahab, H.S., Guedes Soares, C., Pinheiro, L.V., Fortes, C.J.E.M., Santos, J.A., 2021. Experimental and numerical study of wave-induced ship motions and mooring loads of a tanker moored in Leixões port. In: Developments in Maritime Technology and Engineering. https://doi.org/10.1201/9781003216599-36.

Akiyama, H., Shimizu, K., Ueda, S., Kamada, T., 2017a. Investigation on service years of large rubber marine fenders. J. JSCE 5. https://doi.org/10.2208/journalofjsce.5.1_392.

Akiyama, H., Shiomi, T., Omura, A., Yamamoto, S., Ueda, S., Kamada, T., 2017b. Method to estimate the aging of large rubber marine fender. In: Proceedings of the International Offshore and Polar Engineering Conference.

Alvarellos, A., Figuero, A., Carro, H., Costas, R., Sande, J., Guerra, A., Peña, E., Rabuñal, J., 2021. Machine learning based moored ship movement prediction. J. Mar. Sci. Eng. 9 https://doi.org/10.3390/jmse9080800.

Arcadis, 2016a. SHIP-MOORINGS version 10. User Manual.

Arcadis, 2016b. SHIP-MOORINGS version 10. Background Documentation.

Barreras, Hijos de J., 2015. PASSENGER FERRY VESSEL VOLCÁN DEL TEIDE [WWW Document]. URL. http://www.hjbarreras.es/?page=lis-ferries&idp=41.

Bhattacharyya, A., 1943. On a measure of divergence between two statistical populations defined by their probability distribution. Bull. Calcutta Math. Soc. 35, 99–110.

Bhautoo, P.S., 2017. Dynamic mooring analysis to investigate long period wave-induced vessel motions at Esperance Port. In: Australasian Coasts and Ports 2017 Conference.

Bingham, H.B., 2000. A hybrid Boussinesq-panel method for predicting the motion of a moored ship. Coast. Eng. 40 https://doi.org/10.1016/S0378-3839(00)00002-8.

Brodtkorb, P.A., Johannesson, P., Lindgren, G., Rychlik, I., Ryden, J., Sjo, E., 2000. WAFO - a Matlab toolbox for analysis of random waves and loads. In: Proceedings of the International Offshore and Polar Engineering Conference.

Camus, P., Mendez, F.J., Medina, R., Cofiño, A.S., 2011. Analysis of clustering and selection algorithms for the study of multivariate wave climate. Coast. Eng. https://doi.org/10.1016/j.coastaleng.2011.02.003.

IDE Canarias, Government of the Canary Islands, n.D. Viewfinder Grafcan [WWW Document]. URL https://visor.grafcan.es/visorweb/.

Christensen, E.D., Jensen, B., Mortensen, S.B., Hansen, H.F., Kirkegaard, J., 2008. Numerical simulation of ship motion in offshore and harbour areas. In: Proceedings of the International Conference on Offshore Mechanics and Arctic Engineering - OMAE. https://doi.org/10.1115/OMAE2008-57206.

Cid, A., Castanedo, S., Abascal, A.J., Menéndez, M., Medina, R., 2014. A high resolution hindcast of the meteorological sea level component for Southern Europe: the GOS dataset. Clim. Dynam. 43, 2167–2184. https://doi.org/10.1007/s00382-013-2041-0.

Cornett, A., Wijdeven, B., Boeijinga, J., Ostrovsky, O., 2012. 3-D physical model studies of wave agitation and moored ship motions at ashdod port. In: 8th International Conference on Coastal and Port Engineering in Developing Countries. COPEDED, Chennai, India.

Costas, R., Figuero, A., Peña, E., Sande, J., Rosa-Santos, P., 2022a. Integrated approach to assess resonance between basin eigenmodes and moored ship motions with wavelet transform analysis and proposal of operational thresholds. Ocean Eng. 247 https://doi.org/10.1016/j.oceaneng.2022.110678.

Costas, R., Figuero, A., Sande, J., Peña, E., Guerra, A., 2022b. The influence of infragravity waves, wind, and basin resonance on vessel movements and related downtime at the Outer Port of Punta Langosteira, Spain. Appl. Ocean Res. 129, 103370 https://doi.org/10.1016/j.apor.2022.103370.

Cummins, W.E., 1962. The impulse response function and ship motions. Schiffstechnik 57.

de Bont, J., van der Molen, W., van der Lem, J., Ligteringen, H., Mühlestein, D., Howie, M., 2010. CALCULATIONS OF THE MOTIONS OF A SHIP MOORED WITH MOORMASTER™ UNITS.

del Estado, Puertos, de Fomento, Ministerio, 1999. Recommendations for maritime works, Series 3, Planning, management and operation in port areas. ROM 3, 1–99 (-Design of the Maritime Configuration of Ports, Approach Channels and Harbour Basins).

del Estado, Puertos, de Fomento, Ministerio, 2012. Recommendations for Maritime Works, Series 2, Inner Harbor Structures. ROM 2.0 -11 - Recommendations for the Design and Construction of Berthing and Mooring Structures.

Drimer, N., Glozman, M., Stiassnie, M., Zilman, G., 2000. Forecasting the motion of berthed ships in harbors. Int. Work. Water Waves Float. Bodies.

Duarte, T., 2013. SS_Fitting. Theory and User Manual. V5_18-09-2013.

Egbert, G.D., Erofeeva, S.Y., 2002. Efficient inverse modeling of barotropic ocean tides. J. Atmos. Ocean. Technol. 19, 183–204. https://doi.org/10.1175/1520-0426(2002)019<0183:EIMOBO>2.0.CO;2.

Egbert, G.D., Bennett, A.F., Foreman, M.G.G., 1994. TOPEX/POSEIDON tides estimated using a global inverse model. J. Geophys. Res. 99 https://doi.org/10.1029/94jc01894.

Figuero, A., Rodriguez, A., Sande, J., Peña, E., Rabuñal, J.R., 2018. Field measurements of angular motions of a vessel at berth: inertial device application. Control Eng. Appl. Informatics 20.

Figuero, A., Sande, J., Pena, E., Alvarellos, A., Rabunal, J.R., Macineira, E., 2019. Operational thresholds of moored ships at the oil terminal of inner port of A Coruna (Spain). Ocean Eng. 172, 599–613. https://doi.org/10.1016/j.oceaneng.2018.12.031.

Hanson, J.L., Tracy, B.A., Tolman, H.L., Scott, R.D., 2009. Pacific hindcast performance of three numerical wave models. J. Atmos. Ocean. Technol. 26, 1614–1633. https://doi.org/10.1175/2009JTECHO650.1.

Jensen, O.J., Viggosson, G., Thompson, J., Bjordal, S., Lundgren, J., 1990. Criteria for SHIP movements in harbours. Coast. Eng. Proc. 1 https://doi.org/10.9753/icce.v22.%p.

Kwak, M., Pyunan, C., 2014. Evaluation of effective working days considering moored SHIP motion in pohang new harbor. Coast. Eng. Proc. 1 https://doi.org/10.9753/icce.v34.management.20.

Kwak, M., Moon, Y., Pyun, C., 2012. Computer simulation of moored SHIP motion induced by harbor resonance in pohang new harbor. Coast. Eng. Proc. 1 https://doi.org/10.9753/icce.v33.waves.68.

Lewandowski, E.M., 2004. The dynamics of marine craft maneuvering and seakeeping. Ocean Dynam.

Li, S., Qiu, Z., 2016. Prediction and simulation of mooring ship motion based on intelligent algorithm. In: Proceedings of the 28th Chinese Control and Decision Conference. CCDC 2016. https://doi.org/10.1109/CCDC.2016.7531231.

López, M., Iglesias, G., 2014. Long wave effects on a vessel at berth. Appl. Ocean Res. 47 https://doi.org/10.1016/j.apor.2014.03.008.

MarCom Working Group, 2012. Criteria for the (Un)loading of container vessels. PIANC Report 115.

Maritime Research Institute Netherlands (MARIN), 2010. DIFFRAC User Guide, Version 2.0.

Masanganise, J., Magodora, M., Mapuwei, T., Basira, K., 2014. An assessment of CMIP5 global climate model performance using probability density functions and a match metric method. Sci. Insights-An Interantional J. Univers. Res. Publ. 4, 1–8.

Mazzaretto, O.M., Menéndez, M., Lobeto, H., 2022. A global evaluation of the JONSWAP spectra suitability on coastal areas. Ocean Eng. 266, 112756 https://doi.org/10.1016/j.oceaneng.2022.112756.

MetOcean Solutions Ltd, 2018. Wavespectra. GitHub – Metocean/wavespectra.

Molina-Sanchez, R., Campos, Á., de Alfonso, M., de los Santos, F.J., Rodríguez-Rubio, P., Pérez-Rubio, S., Camarero-Orive, A., Álvarez-Fanjul, E., 2020. Assessing operability on berthed ships. common approaches, present and future lines. J. Mar. Sci. Eng. 8 https://doi.org/10.3390/JMSE8040255.

Pinheiro, L.V., Fortes, C., Santos, J., Fernandes, J.L., 2012. Coupling of a boussinesq wave model with a moored SHIP behavior model. Coast. Eng. Proc. 1 https://doi.org/10.9753/icce.v33.waves.69.

Pinheiro, L.V., Fortes, C.J.E.M., Santos, J.A., Fernandes, J.L.M., 2013a. Numerical simulation of the behaviour of a moored ship inside an open coast harbour. In: Computational Methods in Marine Engineering V - Proceedings of the 5th International Conference on Computational Methods in Marine Engineering. MARINE 2013.

Pinheiro, L.V., Santos, J.A., Fortes, C.J.E.M., Fernandes, J.L.M., 2013b. Numerical Software Package SWAMS – Simulation of Wave Action on Moored Ships.

Pinheiro, L., Fortes, C.J., Santos, J.A., Rosa-Santos, P., 2016. Numerical simulation of the motions and forces of a moored ship in Leixões harbour. In: Proceedings of 3rd International Conference on Maritime Technology and Engineering. MARTECH 2016. https://doi.org/10.1201/b21890-31.

Pinkster, J.A., 1980. Low Frequency Second Order Wave Exciting Forces on Floating Structures. Model BASIN, WAGENINGEN, NETHERLANDS, NETHERLANDS Sh, 1980.

Pinto, F.T., Gomes, F.V., Santos, P.R., Soares, C.G., Fonseca, N., Santos, J.A., Moreira, A. P., Costa, P., Dias, E.B., 2008. Analysis of the behavior of moored tankers. In: Proceedings of the International Conference on Offshore Mechanics and Arctic Engineering - OMAE. https://doi.org/10.1115/OMAE2008-58013.

Prpić-Oršić, J., Slapničar, V., Turk, A., 2014. Berth operability estimation related to ship motion. Trans. FAMENA 38.

Romano-Moreno, E., Diaz-Hernandez, G., Lara, J.L., Tomás, A., Jaime, F.F., 2022. Wave downscaling strategies for practical wave agitation studies in harbours. Coast. Eng. 175 https://doi.org/10.1016/j.coastaleng.2022.104140.

Romano-Moreno, E., Diaz-Hernandez, G., Tomás, A., Lara, J.L., 2023. Multimodal harbor wave climate characterization based on wave agitation spectral types. Coast. Eng. 180, 104271 https://doi.org/10.1016/j.coastaleng.2022.104271.

Rosa-Santos, P.J., Taveira-Pinto, F., 2013. Experimental study of solutions to reduce downtime problems in ocean facing ports: the Port of Leixões, Portugal, case study. J. Appl. Water Eng. Res. 1 https://doi.org/10.1080/23249676.2013.831590.

Rosa-Santos, P., Taveira-Pinto, F., Veloso-Gomes, F., 2014. Experimental evaluation of the tension mooring effect on the response of moored ships. Coast. Eng. 85 https://doi.org/10.1016/j.coastaleng.2013.11.012.

Sakakibara, S., Kubo, M., 2008a. Effect of mooring system on moored ship motions and harbour tranquillity. Int. J. Ocean Syst. Manag. 1 https://doi.org/10.1504/IJOSM.2008.017783.

Sakakibara, S., Kubo, M., 2008b. Characteristics of low-frequency motions of ships moored inside ports and harbors on the basis of field observations. Mar. Struct. 21 https://doi.org/10.1016/j.marstruc.2007.11.002.

Sande, J., Figuero, A., Tarrío-Saavedra, J., Peña, E., Alvarellos, A., Rabuñal, J.R., 2019. Application of an Analytic Methodology to Estimate the Movements of Moored Vessels Based on Forecast Data. https://doi.org/10.3390/w11091841. Water (Switzerland) 11.

Shi, X., 2018. A comparative study on the motions of a mooring LNG ship in bimodal spectral waves and wind waves. In: IOP Conference Series: Earth and Environmental Science. https://doi.org/10.1088/1755-1315/189/5/052047.

Simiu, E., Scanlan, R.H., 1996. Wind Effects on Structures: Fundamentals and Applications to Design, third ed. (New York).

Terblanche, L., Van Der Molen, W., 2013. Numerical Modelling of long waves and moored ship motions. In: Coasts and Ports 2013.

Thoresen, C.A., 2003. Port Designer's Handbook: Recommendations and Guidelines. Thomas Telford Publishing. https://doi.org/10.1680/pdhrag.32286.

Trejo, I., Pérez, J.D., Guerra, A., Iribarren, J.R., Gómez, J., Sopelana, J., Peña, E., 2014. Onsite Measurement of Moored Ships Behaviour (RTK GPS), Waves and Long Waves in the Outer Port of A Coruña (Spain). PIANC World Congr. San Fr, USA 2014.

Uzaki, K. ichi, Matsunaga, N., Nishii, Y., Ikehata, Y., 2010. Cause and countermeasure of long-period oscillations of moored ships and the quantification of surge and heave amplitudes. Ocean Eng. 37 https://doi.org/10.1016/j.oceaneng.2009.12.004.

van der Molen, W., 2006. Behaviour of Moored Ships in Harbours.

van der Molen, W., Wenneker, I., 2008. Time-domain calculation of moored ship motions in nonlinear waves. Coast. Eng. 55 https://doi.org/10.1016/j.coastaleng.2008.01.001.

Van Oortmerssen, G., 1976. THE MOTIONS OF A MOORED SHIP IN WAVES. Delft University of Technology.

WAFO-group, 2000. WAFO - A Matlab Toolbox for Analysis of Random Waves and Loads - A Tutorial.

Weiler, O., Dekker, J., 2003. Mooring container ships exposed to long waves. In: Proceedings of the 13th International Harbour Congress, pp. 207–214.

Wenneker, I., Borsboom, M., Pinkster, J., Weiler, O., 2006. A boussinesq-type wave model coupled to a diffraction model to simulate wave-induced SHIP motion. In: 31st PIANC Int. Navig. Congr. 2006. Estoril, Port.

Wichers, J.E.W., 1988. A Simulation Model for a Single Point Moored Tanker. Tech. Univ. Delft. working group PTC II-24, 1995. Criteria for movements of moored ships in harbours: a practical guide (Supplement to bulletin No 88). In: PIANC - Permanent International Association of Navigation Congresses.

Yan, L., 2014. Experimental study of the wharf structure influence on ship mooring conditions. In: Proceedings - 2014 5th International Conference on Intelligent Systems Design and Engineering Applications. ISDEA 2014. https://doi.org/10.1109/ISDEA.2014.110.

Yoneyama, H., Shiraishi, S., Satoh, H., 2004. Experimental verification of a reduction system for low-frequency ship motions and examination for its practical use. In: Ocean '04 - MTS/IEEE Techno-Ocean '04: Bridges across the Oceans - Conference Proceedings. https://doi.org/10.1109/oceans.2004.1405667.